

Dynamics of Orbits near 3:1 Resonance in the Earth-Moon System¹

Donald J. Dichmann², Ryan Lebois³, John P. Carrico, Jr.⁴

Abstract

The Interstellar Boundary Explorer (IBEX) spacecraft is currently in a highly elliptical orbit around Earth with a period near 3:1 resonance with the Moon. Its orbit is oriented so that apogee does not approach the Moon. Simulations show this orbit to be remarkably stable over the next twenty years. This article examines the dynamics of such orbits in the Circular Restricted 3-Body Problem (CR3BP). We look at three types of periodic orbits, each exhibiting a type of symmetry of the CR3BP. For each of the orbit types, we assess the local stability using Floquet analysis. Although not all of the periodic solutions are stable in the mathematical sense, any divergence is so slow as to produce practical stability over several decades. We use Poincaré maps with twenty-year propagations to assess the nonlinear stability of the orbits, where the perturbation magnitudes are related to the orbit uncertainty for the IBEX mission. Finally we show that these orbits belong to a family of orbits connected in a bifurcation diagram that exhibits exchange of stability. The analysis of these families of period orbits provides a valuable starting point for a mission orbit trade study.

Introduction

The Interstellar Boundary Explorer (IBEX) spacecraft is currently in a highly elliptical orbit around Earth near 3:1 resonance with the Moon, with spacecraft apogee oriented to stay away from the Moon. As described in [1-3], this type of orbit would be useful for space weather missions and shows remarkable stability over an interval of several decades.

This article is an extension of [1], which reviews the trajectory trade study for the IBEX extended mission. The goal of this article is to obtain a better understanding of the dynamics of such an orbit, especially its stability. Toward this goal we study the dynamics of near 3:1 resonant periodic orbits, in the CR3BP for the Earth-Moon system. Poincaré recognized the central role of periodic solutions in the structure of a dynamical system [2]. As shown in [1], the actual IBEX orbit is quasi-periodic, not periodic. However it is common for a family of quasi-periodic orbits to exist near a periodic orbit in a Hamiltonian system [3].

¹ Parts of this article appeared in "Lunar-Resonant Trajectory Design for the Interstellar Boundary Explorer (IBEX) Extended Mission", AAS/AIAA Astrodynamics Specialist Conference, Girdwood AK, 2011, AAS-11-454.

² Senior Engineering Specialist, Applied Defense Solutions, 10440 Little Patuxent Parkway, Columbia, MD 21004. Currently Senior Navigation Engineer, Code 595.0, NASA Goddard Space Flight Center, 8800 Greenbelt Road, Greenbelt MD, 20771, donald.j.dichmann@nasa.gov.

³ Aerospace Engineer, Applied Defense Solutions, 10440 Little Patuxent Parkway, Columbia, MD 21004, RLebois@applieddefense.com

⁴ Senior Astrodynamics Specialist, Applied Defense Solutions, 10440 Little Patuxent Parkway, Columbia, MD 21004, JCarrico@applieddefense.com

There have been several fundamental studies of the dynamics of periodic orbits in the CR3BP, including [6-10]. Families of Libration Point Orbits (LPOs) are mapped out in [11-12], and those articles provide extensive literature surveys. Resonant periodic orbits have been studied in [4] and [5]. The significance of resonant orbits in astrodynamics has long been recognized. The works [14-15] discuss resonances in connection with solar system dynamics. Many studies have examined resonance in the dynamics of the asteroid belt, including [16-18]. The search for extrasolar planets has identified systems with pairs of planets that are near resonance, such as [19-20]. During the Apollo era, Broucke [6] computed numerous periodic orbits in the CR3BP of the Earth-Moon system and assessed their stability. There have also been extensive studies of cycler orbits that repeatedly approach the two primary bodies in a system such as the Earth and Moon [22-23]. However, cycler orbits tend to be unstable due to close approaches with the primaries, and so require maneuvers to maintain the periodicity. By contrast, the IBEX orbit requires no orbit maintenance maneuvers for at least ten years. The body of work on resonance orbits like IBEX, which keeps the spacecraft away from the primary bodies, appears to be small but growing. We did not find any orbits in Broucke's catalog [6] similar to the ones studied here. Mathews, McGiffin et al. [24-25] investigated the use of 2:1 resonance orbits with a lunar gravity assist. These two references were used as a basis for the trajectory design of the recently approved Transiting Exoplanet Survey Satellite, to be launched in 2017 [7]. Currently Vaquero and Howell [27-29] are investigating the dynamics of resonant orbits in the Earth-Moon system.

The remainder of this paper is structured as follows.

We first review the orbit properties of the IBEX extended mission. We then summarize the Circular Restricted 3-Body Problem (CR3BP) model. In order to compute periodic solutions of the CR3BP, we exploit the Mirror Theorem [8]. This approach has been used in previous studies, such as [9], to compute LPOs. Based on symmetries in the CR3BP we identify three types of periodic solutions: Planar Mirror, Reflection and Axial. To explore the dynamics of near 3:1 resonant solutions, for each of the orbit types we compute a particular periodic solution with properties similar to the IBEX orbit. These solutions in the CR3BP rotating frame have periods near, but not equal to, the orbit period of the Moon. Because the solution period does not match the Moon's orbit period, the line of apsides of the periodic orbit rotates with a secular rate, which can be useful in science mission observations. For each representative solution, we use Floquet theory to perform a linear stability analysis. We also show how Lyapunov exponents can be computed from Floquet multipliers for a periodic solution. This linear analysis shows that, while the solutions may not be stable in the strict mathematical sense, any growth in perturbations over time is so slow as to make the solution "long-term stable" [10] compared to a typical spacecraft mission lifetime. The Lidov-Kozai mechanism appears to describe a long-term oscillation of orbit inclination and eccentricity observed in the quasi-periodic solutions.

Next we extend the stability analysis to include nonlinear dynamics, using a Poincaré section. A similar analysis for a Mirror solution was performed by Vaquero and Howell in [27-28]. This numerical simulation shows the twenty-year evolution of perturbed solutions, where the perturbation sizes are based on the known uncertainties in orbit determination for IBEX.

While the analysis of three solutions sheds light on the dynamics of near-resonant orbits, the three cases we examine may not be entirely representative. To address this concern, we exploit the Cylinder Theorem for Hamiltonian systems [11] and compute continuous families of Reflection, Axial and Planar Mirror

periodic solutions, and look at the linear stability of each family. Moreover, we show that both the Reflection and the Axial branches connect to the Planar Mirror family in a bifurcation diagram. The computation of the three branches of periodic solutions can provide a rich starting point for a mission trajectory trade study.

To conclude the analysis we take an initial state from the actual IBEX trajectory, and propagate it for twenty years using the CR3BP dynamics. We compare the evolution of the orbit elements under CR3BP dynamics with the evolution under a high-fidelity force model to determine what features of the full dynamics are captured in the CR3BP dynamics. We conclude with some suggestions for future work.

IBEX Extended Mission Orbit Dynamics

The IBEX spacecraft was launched in 2008 into a highly elliptical orbit around the Earth. That orbit experienced significant quasiperiodic oscillations in the perigee radius, due to variations in where the spacecraft encountered the Moon each orbit. IBEX completed its primary mission in January 2011. The project was approved for an extended mission, at which point the project management and science team leads decided to move the spacecraft into a more stable orbit. The Keplerian orbit period varies between about 8.5 and 9.5 days, with an average of 9.13 days. See Figure 1. The period 9.13 days is very close to 3:1 resonance with the Earth-Moon sidereal orbit period of 27.3 days.

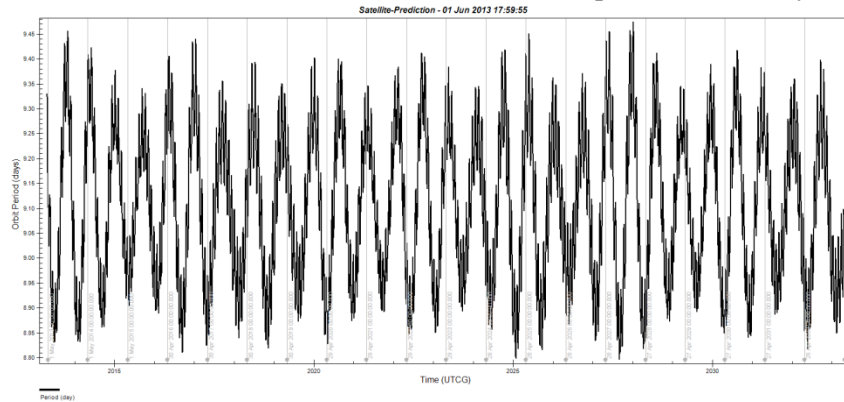


Figure 1. Keplerian orbit period evolution for the IBEX orbit, predicted from Jun 2103 for twenty years of the extended mission orbit.

The IBEX orbit, as of April 2013, is inclined to the lunar orbit plane by about 17 degrees. The orbit has an apogee radius of about 48 Earth radii (Re) and perigee radius of about 10.5 Re. The Keplerian orbit elements vary due to perturbations from lunar and solar gravity, solar radiation pressure and the Earth’s nonspherical shape. Because the Moon has a significant influence on the orbit, it is useful to view the orbit in the Earth-Moon rotating frame. Due to the near resonance, the orbit appears as a three-leaf pattern with apogee near 180 deg or 60 deg from the Moon, as seen in Figure 2.

The IBEX orbit shown in Figure 2 exhibits a quasiperiodic “nodding” motion in the Earth-Moon rotating frame. Figure 1 shows a short-term oscillation corresponding to the orbit period of about 9 days, and a second longer-term oscillation with a period of about 9 months.

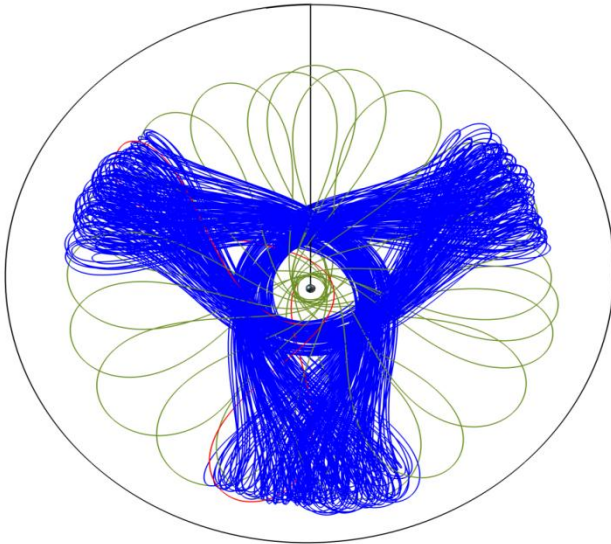


Figure 2. The IBEX orbit viewed in the Earth-Moon rotating frame. In this plot, the Moon is always at the top of the circle. The green curve shows the primary mission orbit, where the spacecraft-Earth-Moon angle varied widely at apogee. The blue curve shows the extended mission orbit, where the spacecraft-Earth-Moon angle remains near 180 deg or 60 deg at apogee. The red curve is the transfer orbit between the primary and extended mission orbits.

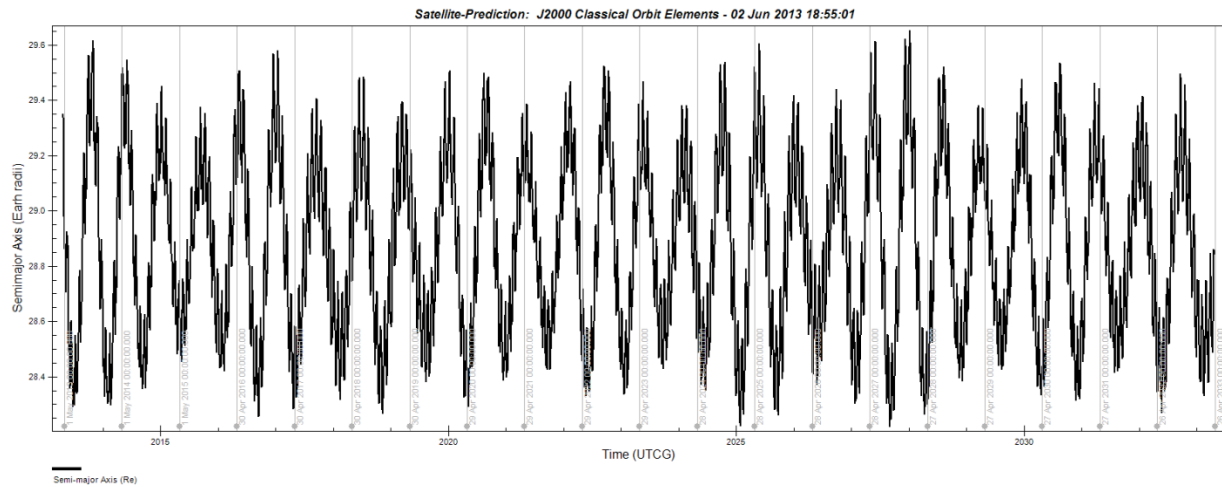


Figure 3. Twenty-year projection of IBEX orbit Keplerian semimajor axis. A critical feature of the stability of this orbit is that the semimajor axis, and so the orbit period, remains steady over a long term, so that the phasing of Moon encounters remains fairly constant.

Figure 3 shows a twenty-year projection of the Keplerian semimajor axis, and exhibits similar oscillations to those observed in Figure 1. A key feature of the long-term stability of the IBEX orbit is that the period and semimajor axis remain fairly steady, oscillating around a stationary average, which means that the orbit apogee maintains regular phasing with respect to the Moon. Figure 4 and Figure 5 show the evolution of perigee radius and inclination to the lunar orbit plane. These two plots exhibit the same 10-month oscillation together with a much longer-term oscillation with a period near 15 years.

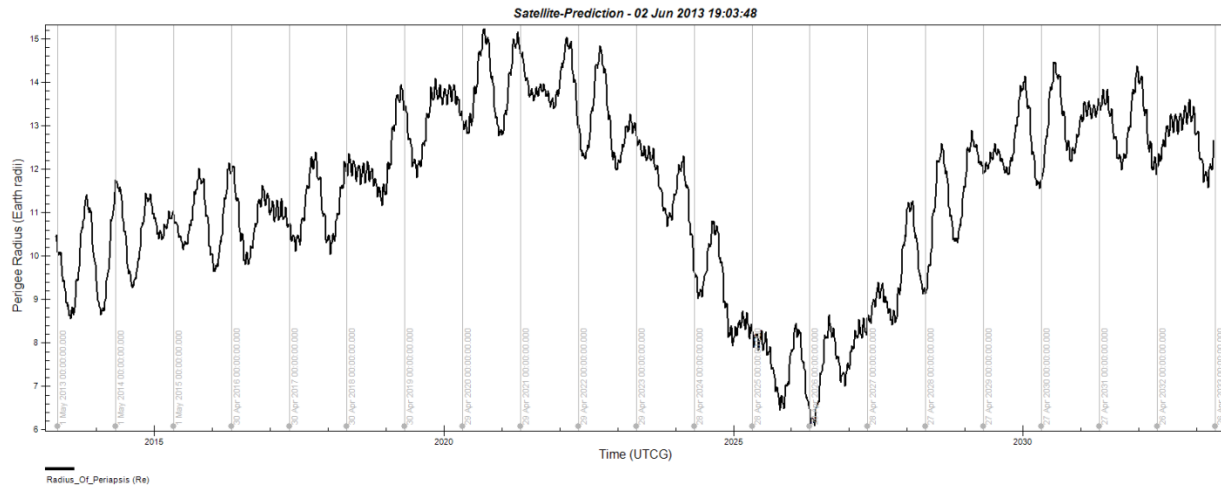


Figure 4. Twenty-year projection of IBEX orbit perigee radius, in Earth radii (Re). This curve exhibits two quasiperiodic oscillations, one with a period of about 9 months, and another with a period of about 15 years.

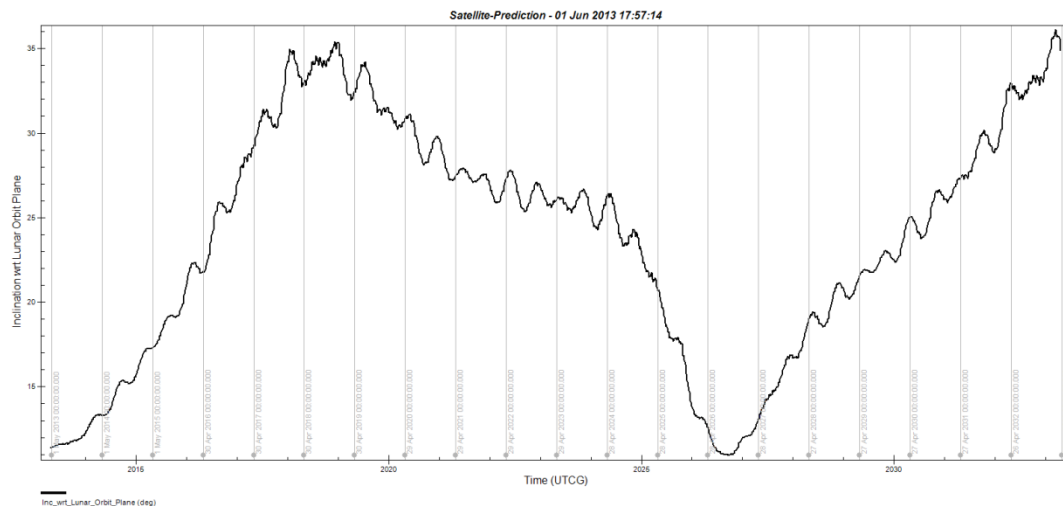


Figure 5. Twenty-year projection of IBEX inclination to the lunar orbit plane, in degrees. This plot exhibits long-term trends similar to those of the perigee radius in Figure 4, with a long-term oscillation period of about 15 years. In particular, both curves exhibit a minimum about June 2026.

In April 2013, the argument of perigee was near 270 deg, so the line of apsides was nearly orthogonal to the line of nodes. The inertial direction of perigee changed at an average rate of about 1 deg per lunar cycle. As noted in [1], this feature is useful in the extended mission because it causes the apogee to move in a direction that fills a gap in IBEX’s observations during its initial two-year mission.

Monte Carlo simulations show that the IBEX extended mission orbit appears stable for decades under perturbations on the order of orbit determination uncertainty [10]. This stability is in sharp contrast to the primary mission orbit, where perigee radius could not be predicted more than a few years into the future [1].

In the remainder of this paper, we study the dynamics of resonant orbits like IBEX in the CR3BP to gain an understanding of the orbit dynamics exhibited in Figure 1 to Figure 5. As we shall show, the CR3BP model does not completely describe the IBEX orbit dynamics but it does provide valuable insights.

Circular Restricted 3-Body Problem

Assume two primary bodies such as the Earth and Moon, each a point mass, orbit each other in circles according to Kepler's laws. A third small body, the spacecraft, is affected gravitationally by the primary bodies but does not affect the orbits of the primaries. Mass is scaled so that the total mass of the primaries is 1, with the mass of the smaller primary equal to μ . For the Earth-Moon system, $\mu = 0.0121505$. Distance is scaled so that the constant distance between the primaries is 1. We assume a distance of 384,400 km between the Earth and Moon.

The CR3BP coordinate system rotates with the primaries, and since distance between them is constant, the two primaries appear stationary. The origin lies at center of mass of the primaries, and the two primaries lie on the x-axis with the larger primary at $-\mu$, the smaller primary at $1 - \mu$. The z-axis points along the orbit normal of the primaries, and the y-axis completes the right-handed orthogonal triad. Time is scaled so that the orbit period of the primaries is 2π . For the Earth-Moon system, the CR3BP time interval 2π corresponds to 27.28 days.

The equations of motion of the CR3BP are

$$\begin{aligned} x' &= v_x \\ y' &= v_y \\ (1) \quad z' &= v_z \\ v_x' &= 2v_y + x - (1 - \mu)(x + \mu)d_1^{-3} - \mu(x - 1 + \mu)d_2^{-3} \\ v_y' &= -2v_x + y - (1 - \mu)yd_1^{-3} - \mu yd_2^{-3} \\ v_z' &= -(1 - \mu)zd_1^{-3} - \mu zd_2^{-3} \end{aligned}$$

where

$$\begin{aligned} d_1 &= \sqrt{(x + \mu)^2 + y^2 + z^2}, \\ d_2 &= \sqrt{(x - 1 + \mu)^2 + y^2 + z^2} \end{aligned}$$

denote the distances to the primaries. (See [12] for a derivation.) Here prime (') denotes a derivative with respect to the CR3BP time variable t . The position vector is $\mathbf{r} = (x, y, z)^T$, where superscript T denotes the transpose, the velocity vector is $\mathbf{v} = (v_x, v_y, v_z)^T$, and the state vector for the system is $\mathbf{s} = (x, y, z, v_x, v_y, v_z)^T$.

The CR3BP system is autonomous: the equations of motion (1) do not explicitly depend on time. The system (1) has one integral of motion, namely the Jacobi integral

$$(2) \quad C(\mathbf{s}) = 2U(x, y, z) - (v_x^2 + v_y^2 + v_z^2)$$

where

$$(3) \quad U(x, y, z) = (x^2 + y^2)/2 + (1 - \mu)d_1^{-1} + \mu d_2^{-1} .$$

The conservation of the Jacobi integral is associated with the Tisserand criterion, which asserts that quantity

$$(4) \quad \frac{1}{2a} + \sqrt{a(1 - e^2)}\cos(i)$$

is nearly constant. (See, for example, [13] , p. 72.) In expression (4), a is the semimajor axis of the orbit, e is the eccentricity, and i is the inclination to the orbit plane of the primaries. We note in the Appendix that the system (1) is a Hamiltonian system, though not in standard form, where the Hamiltonian $H = -C/2$.

In this paper we focus on the computation and analysis of periodic orbits in the CR3BP. The CR3BP has symmetries that can be exploited in the computation of periodic orbits, and a fundamental tool is the Mirror Theorem in [8]. A mirror configuration in the N-body problem is a configuration where each velocity is orthogonal to each position. For the CR3BP there are three important mirror configurations:

- Planar Mirror: The particle lies at position $(x, 0, 0)$ on the x-axis, with velocity $(0, v_y, 0)$ orthogonal to the x-axis and in the $x - y$ plane.
- Reflection: The particle lies at position $(x, 0, z)$ on the $x - z$ plane with velocity $(0, v_y, 0)$ orthogonal to the $x - z$ plane.
- Axial: The particle lies at position $(x, 0, 0)$ on the x-axis with velocity $(0, v_y, v_z)$ orthogonal to the x-axis.

The three resonant families are analogous to more familiar families of LPOs that exhibit the same symmetries [14] [15]:

- Planar Mirror resonant orbits are analogous to Lyapunov LPOs
- Mirror resonant orbits are analogous to Halo LPOs
- Axial resonant orbits are analogous to Axial LPOs

It is shown in the section on Families of Near 3:1 Resonant Orbits that these analogies between resonant orbits and LPOs is also exhibited in the connections between the families in a bifurcation diagram.

The Planar Mirror configuration is actually a special case of both the Reflection and the Axial mirror configurations. The Mirror Theorem asserts that if the solution is in a mirror configuration at time $t = 0$, and in another mirror configuration at $t = T/2$, with $T > 0$, then the solution is periodic with period T . The Mirror Theorem has been exploited in works such as [9] to compute periodic orbits in the CR3BP. For each of the mirror configurations above we compute a type of periodic orbit:

- A Planar Mirror periodic orbit has Planar mirror configurations at its initial point and midpoint. A Planar Mirror periodic orbit is symmetric both under reflection across the $x - z$ plane and under rotation by 180 degrees about the x-axis.

- A Reflection periodic orbit has Reflection mirror configurations at its initial point and midpoint. A Reflection periodic orbit is so named because it is symmetric under reflection across the $x - z$ plane.
- An Axial periodic orbit has Axial mirror configurations at its initial point and midpoint. An Axial periodic orbit is so named because it is symmetric under rotation by 180 degrees about the x -axis.

In this paper the solutions are computed in the rotating CR3BP frame. However for spacecraft mission analysis it is essential to understand the solution properties in an inertial frame: its orientation, its shape, and its evolution. For this purpose we have defined an inertial “EM” frame (for Earth-Moon) with the following properties: The origin of the EM frame is the Earth. The Moon orbits the Earth in a circle in the EM plane. At time $t = 0$, the axes of the inertial EM frame and the rotating CR3BP frame are aligned. Thus at $t = 0$, the Moon lies along the $+x$ axis of the inertial EM frame.

Three Representative Orbits

No single periodic orbit in the CR3BP fully represents the actual IBEX orbit. To gain some understanding of the dynamics of this class of orbits, we first consider a representative example of each of the three types of periodic solutions described above, and then later look at the families of periodic orbits. To compute each periodic solution we employ a differential correction shooting method based on the Mirror Theorem. The shooting method process is adapted to the symmetries of each case. For a Planar Mirror case, the shooting method fixes the initial values of y, z, v_x and v_z at 0, and also fixes the initial value of x . We choose the initial value of x to achieve a desired apogee radius. The estimated period T and the initial value of v_y are allowed to vary to achieve the goals that at time $t = T/2$, the values of y and v_x equal 0. After each step of the differential correction, the estimate of the period T is improved for the updated state by determining the time $T/2$ when the trajectory crosses the $y = 0$ plane.

For the Reflection case, the shooting method is similar to that for the Planar Mirror case but must also handle the z component. The method fixes the initial values of y, v_x and v_z at 0, and also fixes the initial orbit inclination i_0 to the EM plane. The estimated period T together with the initial values of x and v_y are allowed to vary to achieve the goals that at time $t = T/2$, the values of y, v_x and v_z equal 0. The initial value of z is chosen to achieve the initial inclination, given the other initial state components. After each step of the differential correction, the estimate of the period T is improved for the updated state by determining the time $T/2$ when the trajectory crosses the $y = 0$ plane.

For the Axial case, the shooting method fixes the initial values of y, z and v_x at 0, and fixes the initial orbit inclination i_0 . The estimated period T together with the initial values of x and v_y are allowed to vary in order to achieve the goals that at time $t = T/2$, the values of y, z and v_x equal 0. The initial value of v_z is chosen to achieve the initial inclination, given the other initial state components. After each step of the differential correction, the estimate of the period T is improved for the updated state by determining the time $T/2$ when the trajectory crosses the $v_x = 0$ hyperplane. We focus on hyperplane $v_x = 0$ for the Axial case based on its symmetry.

Planar Mirror Case

Figure 6 shows two plots of a Planar Mirror solution for the case where the apogee radius was fixed at 49.95 Earth radii (Re), similar to the IBEX orbit when we performed this analysis in January 2012. The

left plot shows the view in the CR3BP frame while the right plot shows the view in the EM inertial frame. The reflection symmetry of the orbit across the CR3BP $x - z$ plane is apparent in the left plot. The components of the initial state, together with some key parameters, are shown in Table 1. The plot in the CR3BP frame shares the three-leaf structure of the actual IBEX orbit in Figure 2.

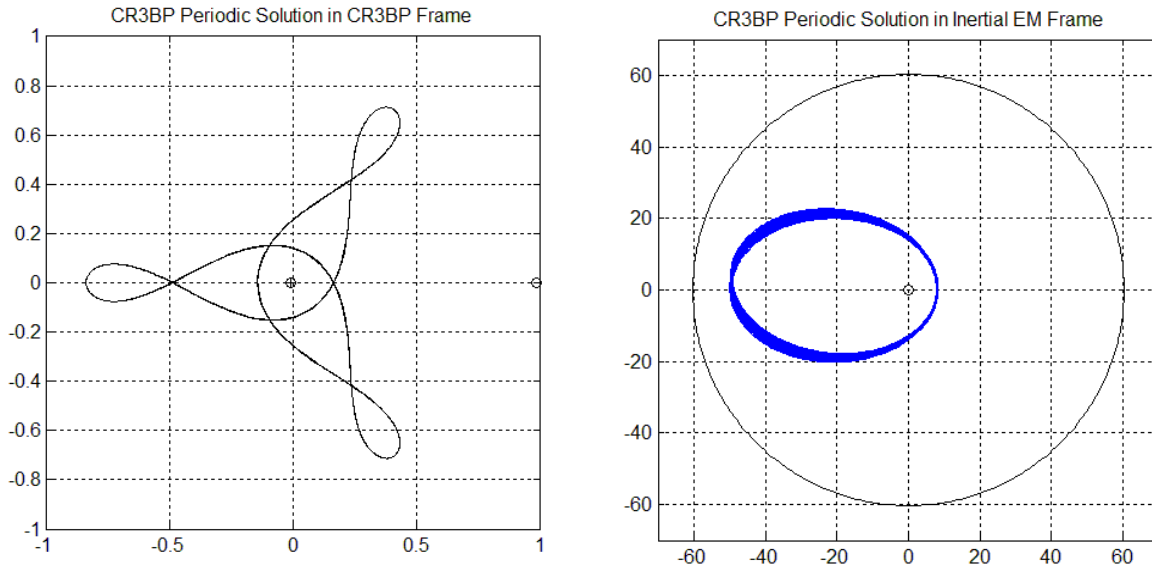


Figure 6. Views of the Planar Mirror periodic orbit. On the left in the solution in the CR3BP frame. Note the mirror symmetry across the x axis. On the right is the orbit in the inertial EM frame. Because the orbit period is not the same as the orbit period of the primary bodies, the orbit in the inertial frame is not periodic. The inertial plot shows evolution over one year.

During the design of the IBEX orbit, one goal was to have the line of apsides rotate in a desired direction, so that the observations would cover a direction in space not covered during the initial two-year mission. It is apparent in the right plot in Figure 6 that the line of apsides rotates in inertial space. A critical factor in the apsidal rotation is the difference between the orbit period T in the CR3BP time unit and the orbit period 2π of the primary bodies. Figure 7 illustrates this concept. For example, the Planar Mirror orbit considered here has an orbit period of $T = 6.2746$, slightly less than 2π . After one satellite orbit period T in the CR3BP frame, the satellite is again at apogee and is in opposition with the Moon. Now consider what happens after one orbit period T in the inertial frame. In Figure 7, the spacecraft and Moon are both located on the x -axis. After one orbit period T , the spacecraft goes from one apogee to the next, and the spacecraft and Moon are again in opposition. Poincaré makes a similar observation in [2], Vol. 1, section 39. Because the period T is less than 2π , the Moon does not complete an entire orbit. As a result, the line of apsides rotates clockwise. The average apsidal rate is $T - 2\pi$ radians per lunar cycle. To measure apsidal direction, we define the perigee angle to be the angle from the x -axis to the perigee direction projected into the EM $x - y$ plane. Figure 8 shows the evolution of the perigee angle over time for the Planar Mirror solution computed here.

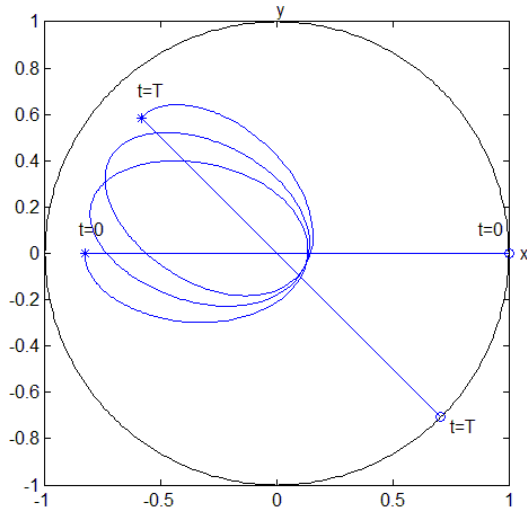


Figure 7. Rotation of the line of apsides in the EM inertial frame for a nearly 3:1 resonant orbit. The Moon (marked by a small circle) follows the black outer orbit, and the spacecraft (marked by an asterisk) follows the blue orbit. At time $t = 0$ the spacecraft is at apogee and is in opposition with the Moon, with both on the x-axis. After one orbit period T in the CR3BP frame, or three orbits in inertial space, the spacecraft is once again at apogee and in opposition with the Moon. In this illustration we assume the period T is less than the Moon's orbit period. Therefore after time T the Moon has not completed a full orbit, so does not lie on the x-axis. Because the spacecraft is in opposition with the Moon at time T , the spacecraft line of apsides must have rotated from its original direction along the x-axis. The angle of rotation per orbit is proportional to the difference between the Moon orbit period and the spacecraft orbit period T . (The angle of rotation is exaggerated for illustration. It would typically be at most a few degrees per period T .)

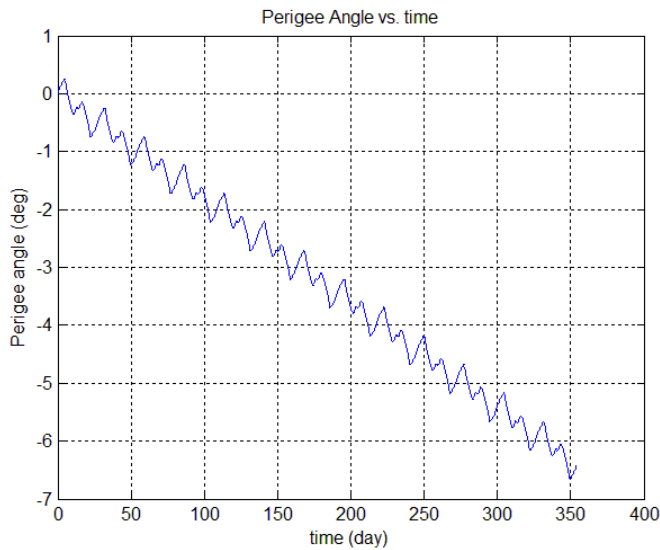


Figure 8. Perigee angle versus time for a near 3:1 EM-resonant orbit over one year. This plot is for a planar orbit with radius of perigee near $8.15 R_e$ which has a period in the CR3BP frame equal to 6.2746. Therefore after one orbit period the Moon is about 0.6 deg short of completing one orbit, and after one year, the perigee angle rotates by about 6.6 deg. In addition to the secular variation, the perigee angle also oscillates each orbit period as the spacecraft-Moon geometry varies.

Reflection Case

Figure 9 and Figure 10 shows a Reflection periodic solution with initial inclination of 23 deg to the EM plane, which is about the average inclination shown in Figure 5 for the predicted IBEX orbit. The initial state components and other parameters are again in Table 1. The CR3BP plot of this solution in Figure 9 exhibits the same three-leaf shape as in Figure 6. However the perigee radius for the Reflection solution is more than $10 R_E$, higher than the perigee radius for the Planar Mirror orbit. Our computations indicate that there is one Reflection solution for each initial inclination. Figure 9 shows the projection of the orbit into the $x - y$ plane, while Figure 10 shows a skew view in three dimensions. In the CR3BP frame, the near 3:1 resonant orbit looks similar to a three-petal flower. In the inertial EM frame, the initial line of nodes is along the y -axis.

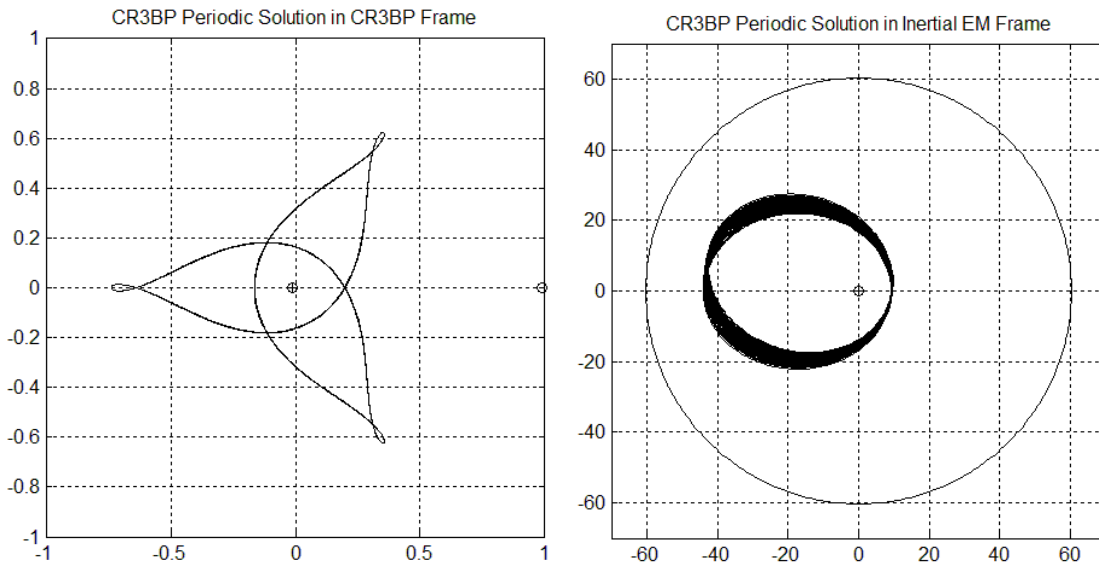


Figure 9. Views of the Reflection periodic orbit in CR3BP and inertial EM frame, projected into the xy -plane.

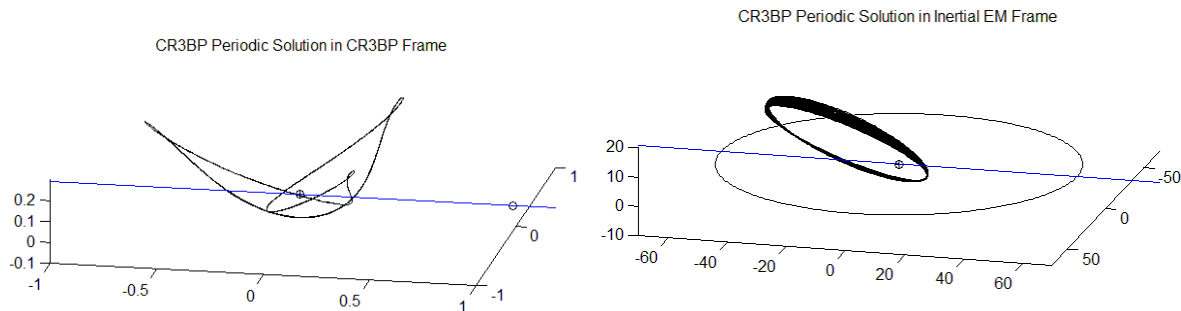


Figure 10. Skew views of the Reflection periodic orbit in CR3BP and inertial EM frame, projected into the xy -plane. The inertial EM frame on the right emphasizes the inclination of the spacecraft orbit to the Moon orbit.

Axial Case

Figure 11 and Figure 12 show the Axial solution for initial inclination 23 deg. As shown in the skew view in Figure 12, an Axial solution in the CR3BP frame has a shape like a three-blade propeller. It can be difficult to see in a single skew view, but the Axial solution is symmetric under a rotation by 180 deg about the x-axis. (The 3:1 resonant solution is also symmetric under a rotation by 120 deg about the z-axis. However the x-axis symmetry is a fundamental symmetry of the dynamics.) The view in the EM inertial frame shows that the initial line of nodes lies along the x-axis.

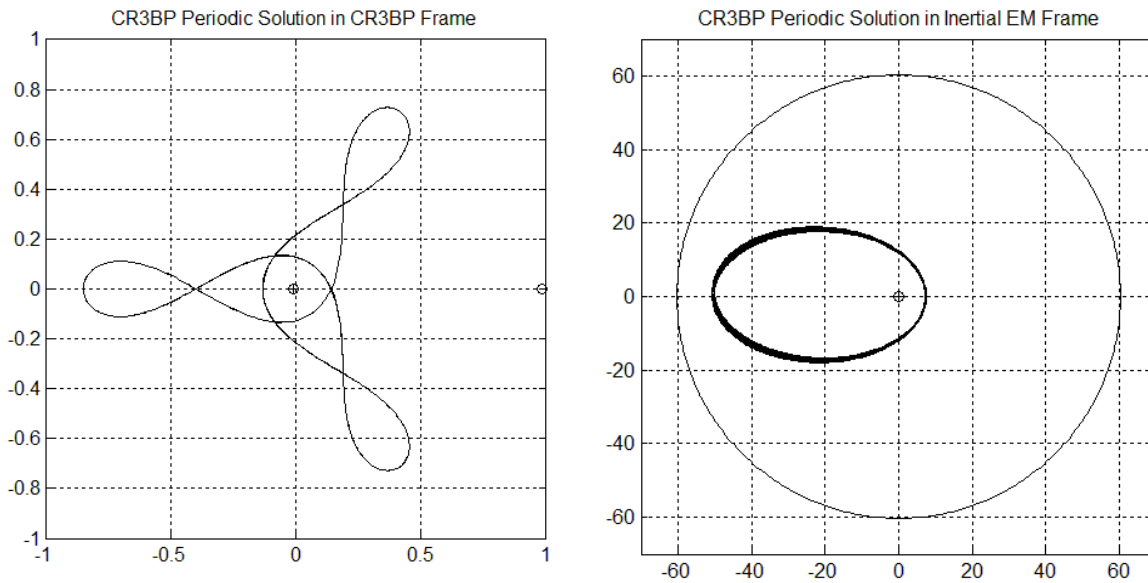


Figure 11. Views of the Axial solution, projected into xy plane

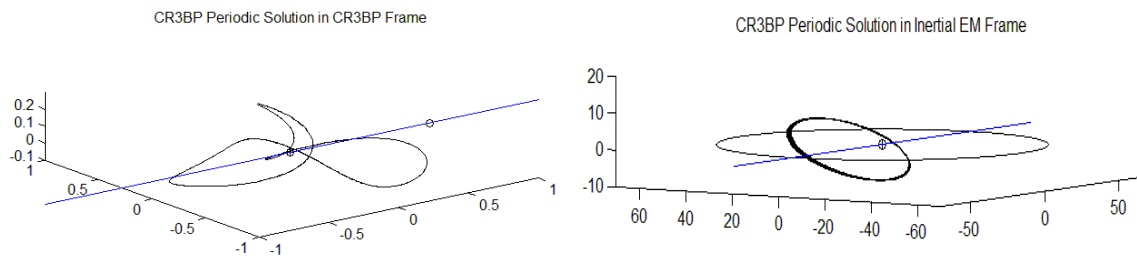


Figure 12. Skew views of the Axial solution. In the CR3BP frame on left, the 3:1 resonant Axial solution resembles a 3-blade propeller. In the EM frame on right, the orbit is inclined to the xy plane with the apsides essentially along the x-axis.

Local Stability Analysis

This study was undertaken to comprehend the apparent stability of the near-resonant orbits like the IBEX orbit. There are numerous types of stability defined in dynamical systems, including asymptotic, linear, orbital and spectral stability. See, for example, [11] and [34-35]. To study the local stability of a solution we linearize the dynamics around the solution. The CR3BP is autonomous, and the solution is periodic with period T , so the linearization about the reference periodic orbit is periodic with period T . Floquet

theory shows that, to assess the stability of the reference orbit, it is sufficient to examine the monodromy matrix \mathbf{M} , which is the state transition matrix $\Phi(T)$ for the time interval T [16].

	Planar Mirror Solution	Reflection Solution	Axial Solution
CR3BP x	-0.84094370	-0.74257943	-0.85249293
CR3BP y	0	0	0
CR3BP z	0	0.31004867	0
CR3BP v_x	0	0	0
CR3BP v_y	0.25043310	0.06950217	0.33447503
CR3BP v_z	0	0	-0.21472796
CR3BP period	6.27459754	6.26105536	6.27964378
Period (days)	27.24731418	27.18850753	27.26922740
Jacobi integral	3.04158388	3.05024235	2.93303141
Initial Apogee Radius (Re)	49.95	47.82	50.64
Initial Perigee Radius (deg)	8.15	10.18	7.46
Initial inclination (deg)	0.00	23.00	23.00
Floquet Multiplier 1	1.0000	1.0000	1.0000
Floquet Multiplier 2	1.0000	1.0000	1.0000
Floquet Multiplier 3	0.7172 - 0.6968i	0.8097 - 0.5868i	0.7194 - 0.6946i
Floquet Multiplier 4	0.7172 + 0.6968i	0.8097 + 0.5868i	0.7194 + 0.6946i
Floquet Multiplier 5	0.9922	0.9997 - 0.0227i	0.9907
Floquet Multiplier 6	1.0078	0.9997 + 0.0227i	1.0094
Period of first quasiperiodic mode Q1 (days)	222.0	272.4	223.1
Period of second quasiperiodic mode Q2 (days)	---	6167	---
Time for unstable mode U to grow by factor of 10 (days)	8090	--	6719

Table 1. Initial states for three representative periodic orbits, with additional dynamical data. Each solution has a pair of Floquet multipliers equal to +1, and a complex conjugate pair with magnitude 1 corresponding to a quasiperiodic mode. The Reflection solution has a second complex conjugate pair, while the Planar Mirror and the Axial each have a real inverse pair. For each quasiperiodic pair, the corresponding period is shown, whereas for each unstable mode, the time to grow by a factor of 10 is shown. In all three cases, the final pair is very close to 1, yielding either a very long period oscillation or a very slow growing instability.

Because the CR3BP system is Hamiltonian, the monodromy matrix \mathbf{M} has some special properties, discussed in the Appendix. For stability analysis the eigenvalues of \mathbf{M} , called the Floquet multipliers, play a critical role. The enumeration of possible configurations of Floquet multipliers in the CR3BP is described in [17] (p. 157 and p. 173), [16] and [18]. In this study we encounter three configurations:

- A pair of values +1
- A complex conjugate pair λ and $\bar{\lambda}$, each with magnitude 1
- A real pair of inverses λ and $1/\lambda$, so the product is 1.

In an autonomous Hamiltonian system the determinant of \mathbf{M} , which is the product of eigenvalues, must equal 1. For a periodic solution in a Hamiltonian system, there must be a pair of Floquet multipliers equal to +1. Moreover, as noted in the Appendix, one eigenvector corresponding to eigenvalue +1 is the right hand side of the differential equation (1) evaluated at the initial state. Floquet multipliers measure how perturbation components called Floquet modes evolve. If a Floquet multiplier λ corresponds to eigenvector \mathbf{v} , and the periodic solution is perturbed by the amount $\varepsilon \mathbf{v}$, then linear analysis predicts that

after m orbit periods the perturbation becomes $\lambda^m \varepsilon \mathbf{v}$. Thus if a Floquet multiplier has magnitude greater than 1, then that Floquet mode grows exponentially, and the solution is unstable. However, among the solutions studied here, when there does exist an unstable Floquet multiplier then it is only slightly larger than 1, and the growth in the unstable direction can take decades to reach a significant size. In an autonomous Hamiltonian system, the Hamiltonian is conserved and phase space volume is conserved, so a solution cannot be asymptotically stable. If all of the Floquet multipliers have magnitude 1, then the solution is called *spectrally* stable. If in addition there is a complete set of eigenvectors, then the solution is *linearly* stable [11].

In the deficient case where the pair of eigenvalues $+1$ have only one eigenvector, the Jordan canonical form of \mathbf{M} is not diagonalizable and contains a 2-by-2 block with diagonals $+1$, and there is an associated generalized eigenvector. Weisel and Pohlen [18] showed that this situation occurs when the periodic solution is part of a continuous family of periodic solutions, and the period varies with an integral of motion. A familiar example of deficiency is Keplerian motion where the orbit period depends on the semimajor axis. In this situation, the periodic solution itself is not stable. (Suppose that a spacecraft is placed in a circular orbit, and a second spacecraft is placed in a slightly higher circular orbit near the first satellite. Because the second satellite has a longer orbit period it drifts away from the first satellite in the along-track direction, initially at a linear rate.) This is a very mild sort of instability, where the separation rate is only linear in time. Although the two solutions drift apart, their two orbits may remain close together, a phenomenon called *orbital* stability. (See [19], p. 274.)

Figure 27 shows that each of the periodic solutions studied here is in fact part of a family where the period varies with Jacobi integral, so the Jordan block with eigenvalue $+1$ is not diagonalizable. For each periodic solution we computed the Jordan canonical form of \mathbf{M} using the Matlab function *eig* . However, the numerical errors inherent in finite-precision calculations make it challenging to detect eigenvector degeneracy. Instead *eig* produces a pair of distinct, approximate eigenvalues near $+1$. The Appendix describes a way to use the Matlab results to obtain the Jordan canonical form.

In the eigenvalue decomposition of each periodic solution we also find at least one complex conjugate pair with magnitude 1, corresponding to a quasiperiodic mode. For such a pair it is useful to convert to a real Jordan block form in a standard way [20]: A pair of eigenvalues $\alpha \pm i\beta$ in the complex Jordan canonical form yields a 2-by-2 real Jordan block of the form

$$\begin{pmatrix} \alpha & -\beta \\ \beta & \alpha \end{pmatrix}$$

The corresponding vectors, the Floquet modes, are the real and imaginary parts of the eigenvectors. Floquet modes can be used to control motion around a periodic solution based on the natural dynamics. See, for example [21].

The result of the Floquet analysis for each of the three types of periodic solutions is summarized in Table 1. The three solutions have similar Floquet structures.

- A pair of multipliers $+1$, with modes labeled P1a and P1b:

- P1a lies along the eigenvector which is the time derivative of the state, given by equation (1). This corresponds to translation along the periodic solution, so the perturbation does not grow over time.
- P1b lies along the generalized eigenvector. Perturbation along this direction produces a small change in Jacobi integral and a slightly different period. The perturbed orbit is nearly the same as the nominal periodic solution. However the perturbed solution drifts away from the periodic solution linearly in time.
- A complex conjugate pair of multipliers with magnitude 1, with modes Q1a and Q1b:
 - This produces a quasiperiodic oscillation about the periodic solution. A complex multiplier $\lambda = \alpha + i\beta$ yields a rotation of angle $\theta = \text{atan2}(\beta, \alpha)$ radians about the periodic solution each orbit period. The oscillation period is therefore $2\pi T/\theta$. For the Planar Mirror, Axial and Reflection solutions, the oscillation periods for this mode are 222, 223 and 262 days, respectively.

The Reflection solution has a second pair of quasiperiodic modes Q2a and Q2b with a very long period of 6167 days or 16.88 years. Thus the Reflection solution is spectrally stable. In contrast, the Planar Mirror and the Axial solutions have a stable mode S and an unstable mode U corresponding to a real inverse pair of Floquet multipliers close to 1. For the Planar Mirror solution, the stable and unstable modes are both in the z direction, so that in-plane motion is spectrally stable. Despite this distinction between the long-term dynamics of the Reflection solution versus the Planar and Axial solutions, the Floquet multipliers in the third pair for all of these solutions are all close to +1. Numerical results below show that a very long-period oscillation and a slowly growing unstable mode appear very similar for many years.

Floquet Modes of the Planar Mirror Solution

To understand more deeply the dynamics near each solution, we applied perturbations in each of the Floquet modes and propagated each perturbed solution for twenty years. As a reference we used a perturbation scale of $\sigma = 1e - 5$ in the CR3BP components. This corresponds to perturbations of 3.8 km in position, and $1e-5$ km/sec in velocity. These values are close to the standard deviations in orbit determination solutions for IBEX at apogee. For example, Figure 13 shows the quasiperiodic solution produced when we perturb the Planar solution by $10,000 \sigma$ along the quasiperiodic Floquet mode Q1. This quasiperiodic solution looks similar to the IBEX orbit shown in Figure 2.

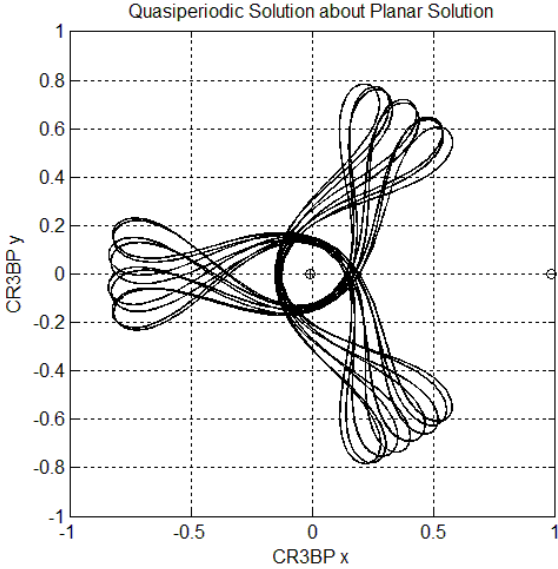


Figure 13. Quasiperiodic solution produced by perturbing the Planar Mirror periodic solution along the first oscillatory Q1 mode. This quasiperiodic solution is obtained from a perturbation in the Q1 component with magnitude $10,000 \sigma$.

In most of our simulations, the perturbation magnitude is 1000σ , except where noted. Figure 14 shows the variations in semimajor axis for the various modes. The right plot in Figure 14 clearly exhibits the quasiperiodic oscillations with period around 222 days. The left plot shows that in the unstable mode (red curve), the oscillation in the semimajor axis grows slightly over twenty years from about 25 km to 50 km. However, even in the unstable mode, the average value of semimajor axis remains the same, so that the phasing of encounters with the Moon remains about the same. By contrast, Figure 15 and Figure 16 show that the unstable mode does cause the perigee radius and inclination to change over time. For the Planar solution, Table 1 shows that the largest Floquet multiplier is 1.0078. We propagate for 20 years or 267.6 lunar cycles. Thus we would expect the perturbation in the unstable mode to multiply by a factor of $1.0078^{267.6} = 8.00$, and the stable mode to multiply by a factor of $1/8.00 = 0.125$. Figure 15 is consistent with those values. There is a much slower growth in the oscillation of the semimajor axis, shown in Figure 14. These plots show the evolution of a perturbation in the individual Floquet modes. A random perturbation in the initial state would be a linear combination of the Floquet modes. Thus, only a portion of the initial perturbation would be in the unstable direction. Moreover, another component of the perturbation would be in the stable direction, and its decay would mitigate the growth due to the unstable direction. Thus we would expect the typical growth rate to be slower than the unstable mode alone would predict, at least until the stable component has decayed to near 0.

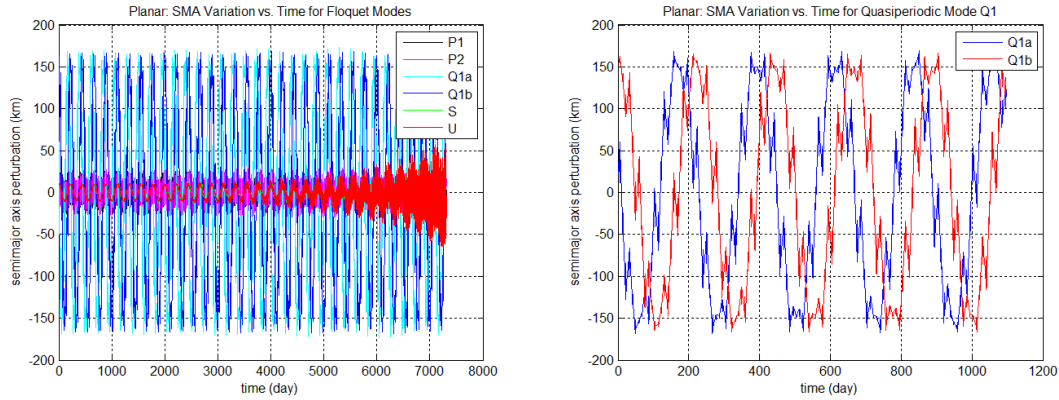


Figure 14. Variation in semimajor axis for Planar solution, under perturbations in the Floquet modes with magnitude 1000σ . The plot on the right shows the evolution of mode Q1 for the first three years, and more clearly exhibits the period near 220 days.

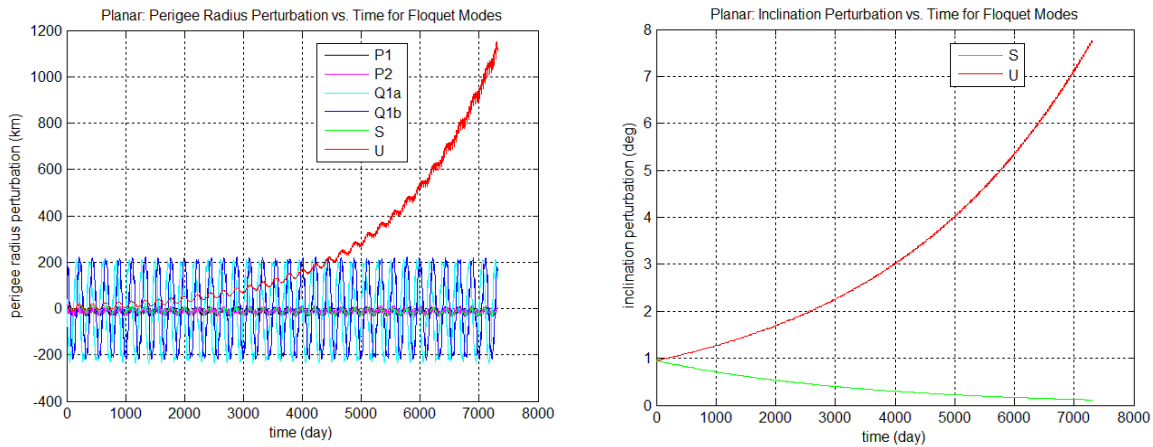


Figure 15. Variations in perigee radius (left) and inclination (right) for Planar solution, for perturbations with magnitude 1000σ . The unstable mode causes the most significant change in perigee radius. For inclination, only the stable and unstable modes are shown since the other modes do not affect out-of-plane motion.

To gain a better understanding of the effect of perturbation magnitude, we ran simulations with magnitudes 100σ , 1000σ and $10,000 \sigma$. Some of the results are shown in Figure 16. For magnitudes 100σ and 1000σ we observe exponential growth in perigee radius and in inclination for the twenty-year duration of the simulation. It is noteworthy that for amplitude $10,000 \sigma$, the growth in perigee radius and in inclination perturbation appears exponential at first, but then levels off after about 16 years. This behavior may be associated with the Tisserand criterion (4), which together with the preservation of semimajor axis puts bounds on the range of eccentricity and inclination values. It was also found that if we apply a perturbation magnitude of about $22,000 \sigma$ in the quasiperiodic mode Q1, the oscillations like those seen in Figure 13 become so large that the orbit apogee gets close to the Moon, disrupting the resonance and producing a chaotic orbit.

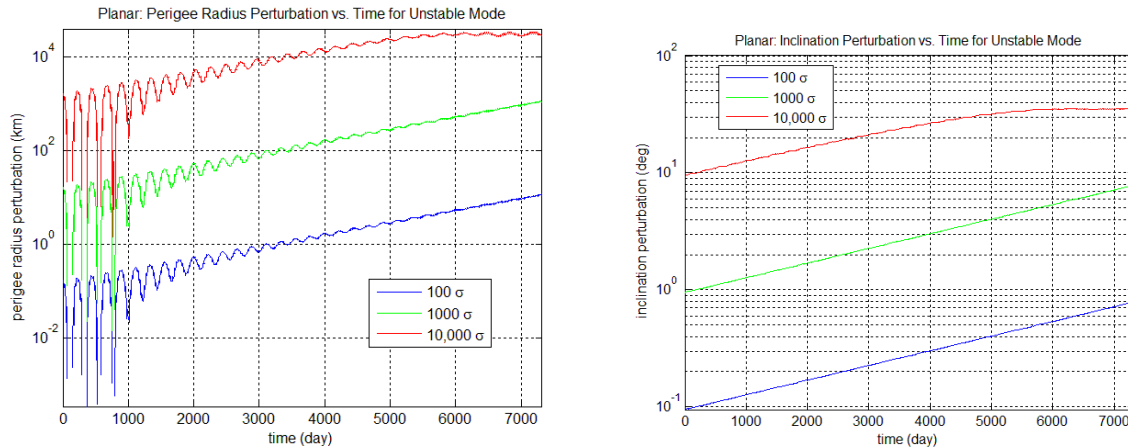


Figure 16. Variations in perigee radius (left) and inclination (right) for different perturbation magnitudes. The vertical axis in each plot uses a logarithmic scale, so a linear trend in the curve indicates exponential growth. For perturbation magnitude 10,000 σ , both perigee radius and inclination appear to level off and remain bounded.

Figures 14, 15 and 16 have several characteristics similar to the projected IBEX orbit shown in Figures 3, 4 and 5, with some notable differences. The semimajor axis maintains an essentially constant average in both cases. The perigee radius and the inclination show an oscillation on the order of months, although the oscillation period shown for IBEX is slightly longer than the 222-day oscillation period for the Planar solution. The perturbed Planar solution also shows long-term growth, on the time scale of ten to twenty years. For initial perturbations on the scale of 10,000 σ , the perturbation remains bounded, just as the IBEX oscillations remain bounded in this time frame.

Floquet Modes of the Reflection Solution

In this section we examine the Floquet modes for the Reflection solution, using much the same analysis as for the Planar solution. The key distinction is that the Reflection solution has a second quasiperiodic mode Q2, with a period of 16.88 years, instead of the stable/unstable mode pair for the Planar solution. The second quasiperiodic mode is apparent in Figures 17 and 18 plotting the evolution of perigee radius and inclination. Even when the perturbation magnitude is increased to 10,000 σ in Figure 19, the long-term oscillation persists. The evolution of orbit elements for the Reflection solution, with the three periods on the scale of 9 days, 10 months and 17 years, is qualitatively very similar to the IBEX orbit evolution, even though the two orbits have significantly different initial perigee radius values.

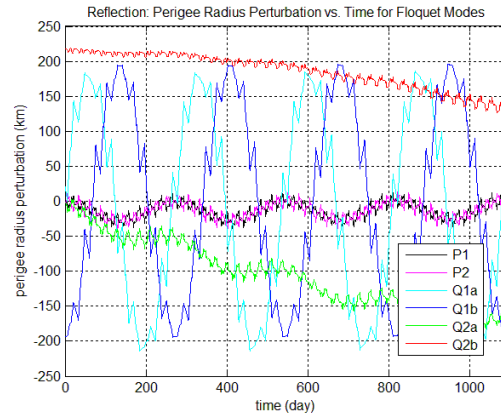
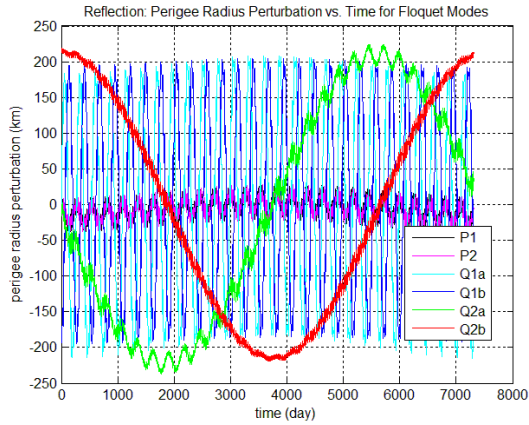


Figure 17. Variation in perigee radius for the Reflection solution. The plot on the left shows that the quasiperiodic mode Q2 oscillates with period near 17 years, as predicted. The plot on the right focuses on the initial 3-year interval, and shows more clearly the variations due to mode Q1 with period near 270 days.

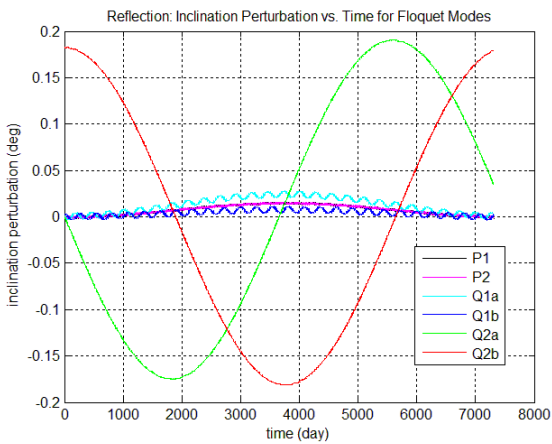


Figure 18. Variations in inclination for Reflection solution. Note the Q2 variations in particular, which appears to be in phase with the perigee radius in Figure 17.

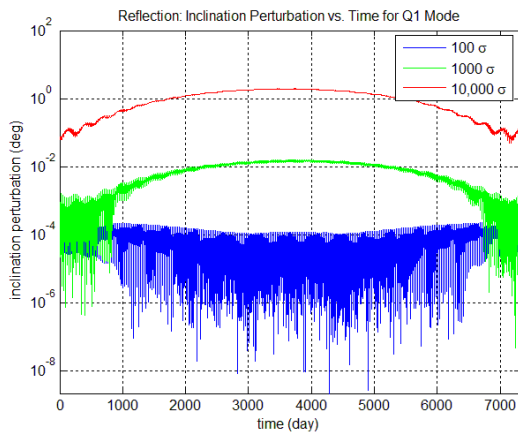


Figure 19. Variation in inclination for Reflection solution, for various perturbation magnitudes. As in Figure 16, we use a logarithmic scale to capture the wide range of values. Although the initial perturbation is in the Q1 mode, the oscillation for magnitude 10,000 σ exhibits a 17-year period, like the Q2 mode.

Floquet Modes of Axial Solution

The Floquet modes of the Axial solutions are similar to those for the Planar solution, but there are some distinct differences. In Figure 20, the average semimajor axis value stays essential constant, as with the Planar case. However, for the Axial unstable mode, the growth in the oscillation magnitude is closer to the factor of $1.0094^{267.6} = 12.23$ predicted by linear theory.

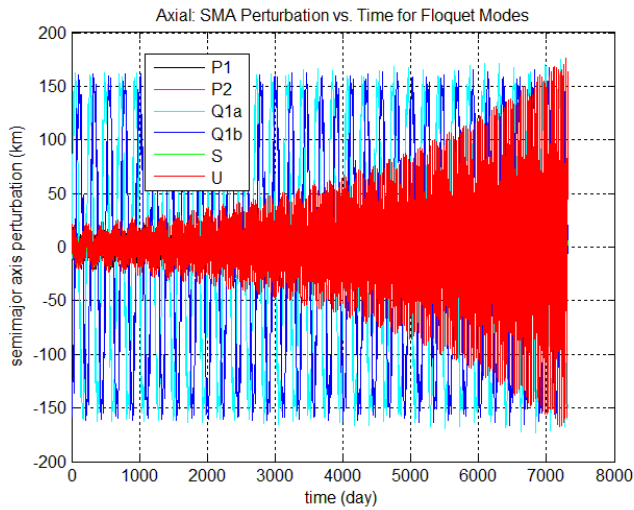


Figure 20. Variation is semimajor axis for Axial solution. Note in particular the growth in the oscillation magnitude for the unstable mode, although the average value remains nearly constant.

Figure 21 shows that for the Axial solution, the unstable mode causes both the perigee radius and the inclination to decrease, in contrast to the Planar solution where both increase. The two solutions share the nonlinear behavior that for an initial perturbation magnitude of $10,000 \sigma$, the perturbation initially grows then remains bounded. In Figure 22, the perturbation in the U mode for the Axial solution appears to behave as a long-period oscillation. That behavior is similar to what we see for the IBEX orbit in Figure 4 and Figure 5.

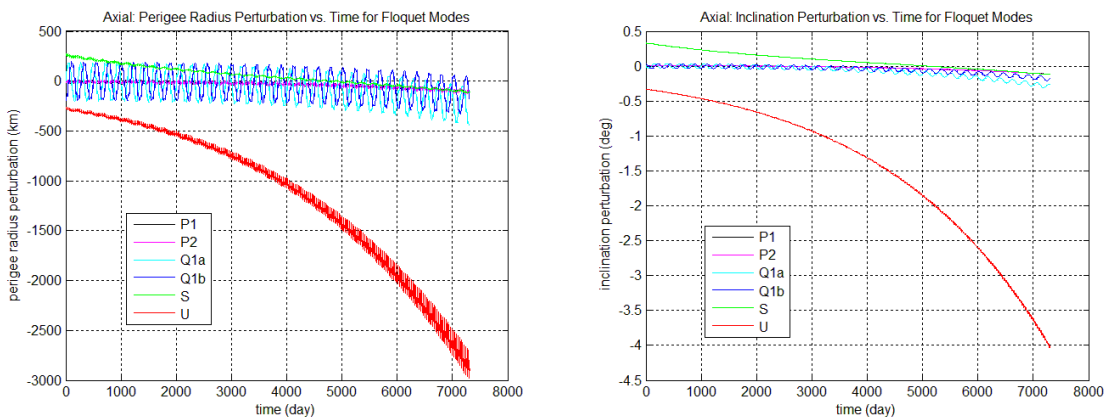


Figure 21. Variation in perigee radius (left) and inclination (right) for Axial solution.

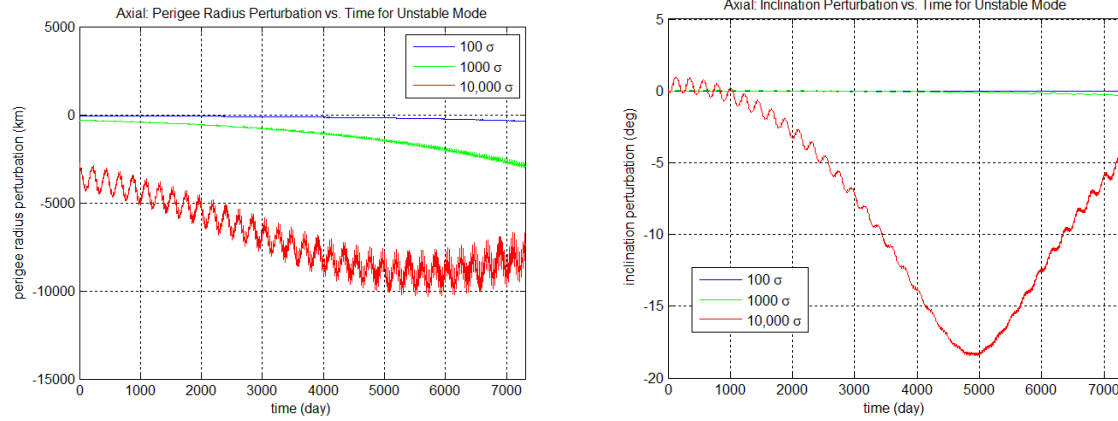


Figure 22. Variation in perigee radius (left) and inclination (right) for Axial solution, for various perturbation magnitudes. For the magnitude 10,000 sigma, the perturbation appears to remain bounded over decades.

Another way to measure the time rate of change of perturbations, closely related to the Floquet multiplier, is the Lyapunov exponent. A Lyapunov exponent is a more general tool than a Floquet multiplier, because a Lyapunov exponent can be computed for a nonperiodic solution. Let $\{m_j(t)\}$, $j = 1$ to 6, be the eigenvalues of the state transition matrix $\Phi(t, \mathbf{s}_0)$ for a given initial state \mathbf{s}_0 . Then the Lyapunov exponents λ_j are defined by

$$(5) \quad \lambda_j = \lim_{t \rightarrow \infty} \frac{1}{t} \ln(m_j(t))$$

when the limit exist. (See [22], p. 67.) For a periodic solution with initial state \mathbf{s}_0 and period T , let $\{\mu_j\}$ be the Floquet multipliers, i.e. the eigenvalues of the monodromy matrix $\mathbf{M} = \Phi(T, \mathbf{s}_0)$. It follows that $\mathbf{M}^k = \Phi(kT, \mathbf{s}_0)$, so $m_j(kT) = \mu_j^k$ for $k = 0, 1, 2, \dots$. We can use these observations in equation (5) to show that the Lyapunov exponents for a periodic solution are related to the Floquet multipliers by

$$(6) \quad \mu_j = \exp(\lambda_j T), j = 1 \text{ to } 6$$

(See [22], p. 68.) In this study we used the Lyapunov exponents associated with the quasiperiodic modes to compute the oscillation periods.

Nonlinear Stability Assessment using Poincaré Maps

The stability analysis to this point has been based on the linearized Floquet analysis. For a more thorough assessment of the stability we must consider a variety of perturbations. The Poincaré map is a tool that, like Floquet analysis, allows us to reduce the dynamics to a discrete-time mapping [22]. In a Poincaré map we first define a Poincaré section, which is a five-dimensional hypersurface in the six-dimensional state space. For the map we record the discrete points where each trajectory crosses the Poincaré section. Like the differential correction methods described above, we selected the Poincaré section to suit the periodic solution. For the Planar Mirror and the Reflection solutions, we used the hyperplane $y = 0$ as the Poincaré section. For the Axial solution, we used the hyperplane $v_x = 0$. We then generated a set of random perturbations from the initial state of the periodic solution, propagated the perturbed solution for

twenty years, and recorded the Poincaré section crossings. Each of the six components of each perturbation was a random draw from a normal distribution with mean zero and a fixed standard deviation: 150 draws with standard deviation 100σ , and 150 draws with standard deviation 1000σ . Because we perturb each of the six components, the standard deviation of the state vector perturbation magnitude is $\sqrt{6} = 2.45$ times the standard deviation of each component perturbation. It is common with Poincaré maps to restrict the perturbed states to the same value of Jacobi integral as the nominal solution, and we have done so here. For each random draw we computed the normal to the level set of the Jacobi integral, and iteratively projected the perturbed solution toward the level set of the nominal periodic solution. This “isosurface projection” only required a few iterations for each draw of the initial perturbation.

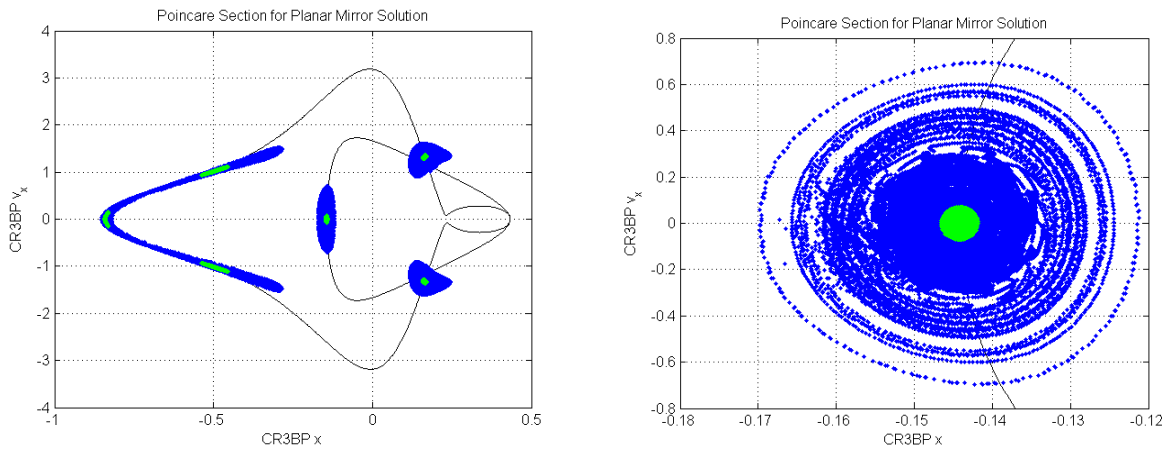


Figure 23. Poincaré map for the Planar Mirror solution. The Poincaré section for this mapping is the hyperplane $y = 0$, and the resulting map is plotted in the $x - v_x$ plane. The black curve represents the Planar Mirror periodic solution, the green dots represent the evolution of perturbations with standard deviation 100σ , while the blue dots represent the evolution of perturbations with standard 1000σ . The distribution of the data points is due primarily to quasi-periodic oscillations. The plot on the right focuses on the region near the center of the left plot.

Figure 23 shows the computed Poincaré map for the Planar Mirror solution, projected into the $x - v_x$ plane. A similar mapping appears in [23]. The black curve shows the Planar Mirror solution, the green dots show the crossings for standard deviation 100σ and the blue dots show the crossings for standard deviation 1000σ . The results indicate stability under large perturbations: The Poincaré map points remain near the nominal solution. The spread of the crossing points is due to the quasiperiodic oscillations. The plot on the right in Figure 23 shows details around the crossing at the middle of the left plot. The ring-like patterns are indicative of the quasiperiodic oscillations.

Figure 24 shows the Poincaré map for the Reflection solution. The patterns are similar to those in Figure 23, but more complex due to the out-of-plane motion. Figure 25 shows the Poincaré map for the Axial solution, projected in the $x - y$ plane, and again indicates effective stability under the perturbations.

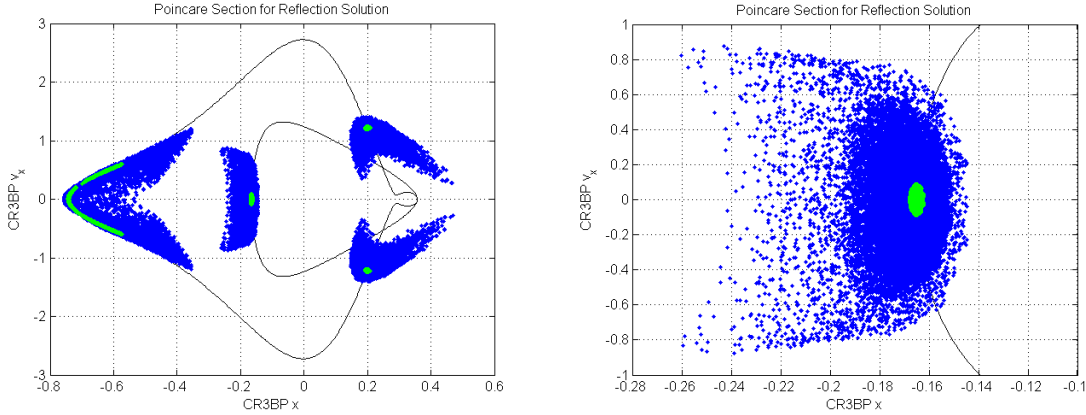


Figure 24. Poincaré map for the Reflection solution.

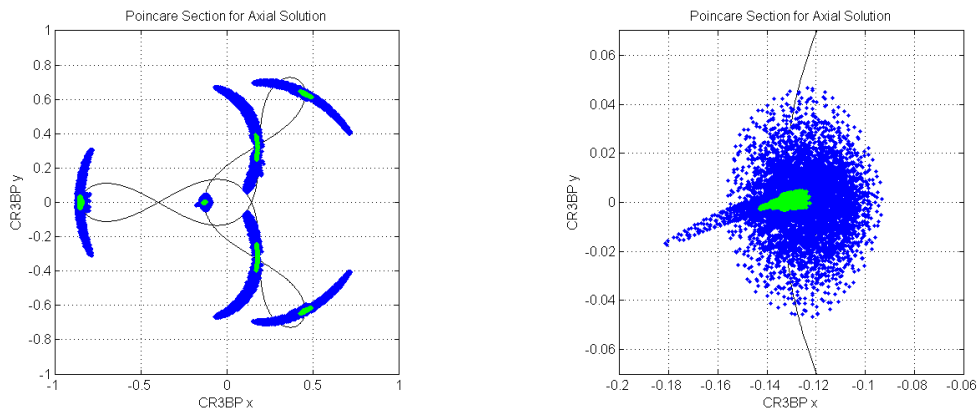


Figure 25. Poincaré map for the Axial solution. The Poincaré section for this mapping is the hyperplane $v_x = 0$, and the map is plotted in the $x - y$ plane. The shape of the region shown in the right plot, with a “spike” protruding to the downward left, suggests that there are two overlapping patterns corresponding to distinct oscillations.

Families of Near 3:1 Resonant Orbits

Thus far we have examined in detail three particular periodic solutions similar to the IBEX orbit. For a deeper understanding of the dynamics we looked at other nearby periodic solutions. A fundamental result in the study of periodic solutions in a Hamiltonian system is the Cylinder Theorem [11], Theorem 6.5.1, p. 82, which states that in generic circumstances a periodic solution lies on a smooth cylinder of periodic solutions parameterized by an integral of motion. Using elementary continuation methods, we generated portions of the Planar Mirror, Reflection and Axial families starting from the particular solutions studied above. Figure 26 shows a projection of these families in a plot of perigee radius vs. inclination. In Figure 26, each point on the three curves represents the initial state of a periodic solution. The particular Planar solution considered above has an initial perigee radius of $8.15 R_e$, while the particular Reflection and Axial solutions are at initial inclination 23 deg. The Reflection family was computed from inclination 0 up to 67 deg, where the perigee radius went below $2 R_e$. For the Axial family we computed the branch

from 0 deg to 81.1 deg inclination, at which point the orbit becomes nearly circular and the initial velocity in the rotating frame becomes nearly vertical. Although the velocity in the rotating frame is nearly vertical, the velocity in the inertial frame is not because the transformation from rotating to inertial frame introduces the term $\boldsymbol{\omega} \times \boldsymbol{r}$ in the velocity. This explains why the inclination in the inertial frame is 81.1 deg, not 90 deg. Figure 26 represents three key families of periodic orbits with apogee away from the Moon, but it is not exhaustive. In particular, the family of Reflection orbits we computed is the branch with perigee above the $x - y$ plane, analogous to the “Northern” branch of halo orbit [9]. There is a symmetric “Southern” branch with perigee below the $x - y$ plane. Similarly the branch of Axial orbits we computed has perigee at the descending node, but there is a symmetric branch with perigee at the ascending node.

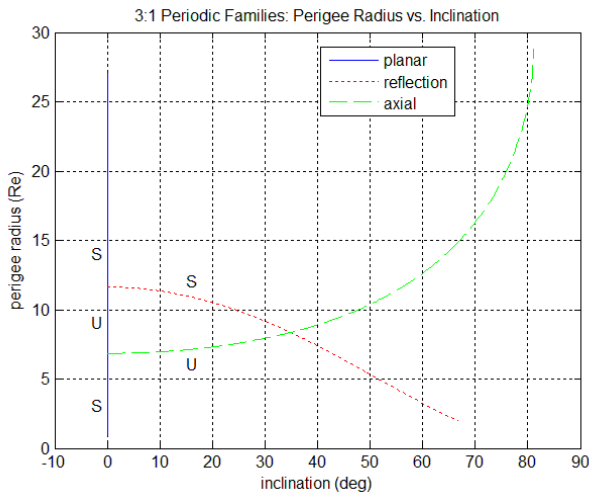


Figure 26. A bifurcation diagram of the families of periodic solutions. A point on each curve represents the initial point of a periodic orbit. The vertical blue line at inclination = 0 represents the Planar orbits with various R_p values. The Reflection orbit family and Axial orbit family each intersect the Planar orbit family, at $R_p = 11.64 R_e$ and at $R_p = 6.85 R_e$, respectively. Although the Reflection and Axial families appear to intersect each other in this two-dimensional projection, they do not actually meet. The S and U labels indicate whether the solutions on a given segment are stable or unstable in the spectral sense.

A significant feature of this diagram is that the Reflection and Axial families each bifurcate from the Planar Mirror family, at different points. The initial states and dynamic properties of the bifurcation points are given in Table 2. Note that each bifurcation point in Table 2 has two pairs of Floquet multipliers +1, showing that it belongs to two families of periodic solutions. In Figure 26 we have labeled segments of the branches with an S or U to indicate respectively whether it is stable or unstable in the spectral sense. In particular, the Planar Mirror solutions are spectrally unstable for perigee radius between 6.85 and 11.64 R_e , but spectrally stable outside that range. It is not uncommon for an exchange of stability to occur at bifurcation points [24], as pairs of eigenvalues merge at +1 then split.

Figure 27 provides another view of the bifurcation diagram, showing the CR3BP orbit period versus Jacobi integral. This diagram shows that the orbit period does vary with the Jacobi integral for each family, so the Floquet multiplier +1 must occur in a 2-by-2 block in the Jordan canonical form [18].

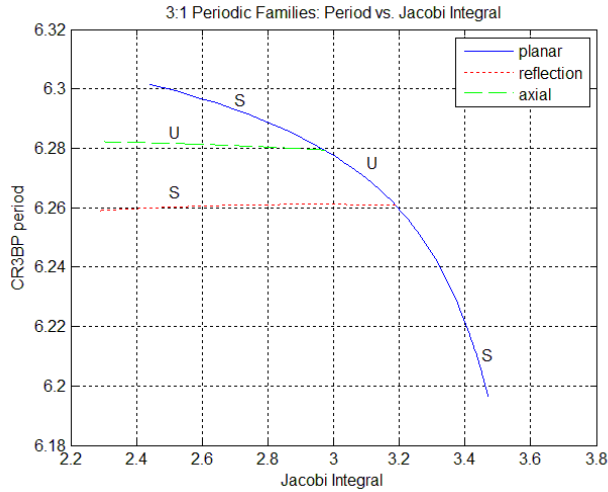


Figure 27. Another view of the bifurcation diagram for periodic families. This plot shows the CR3BP period of the solution vs. the Jacobi integral. For comparison with Figure 26, the highest value of Jacobi integral for the Planar family corresponds to the solution with the largest perigee radius value. For the Reflection and Axial families the period varies slowly with Jacobi integral.

	Branch Point from Planar to Reflection	Branch Point from Planar to Axial
CR3BP x	-0.7821	-0.8628
CR3BP y	0	0
CR3BP z	0.0000	0
CR3BP v_x	0	0
CR3BP v_y	0.0526	0.3274
CR3BP v_z	0	0.0000
CR3BP period	6.2607	6.2794
Period (days)	27.187	27.268
Jacobi Constant	3.1887	2.9729
Initial R_a (Re)	46.40	51.27
Initial R_p (deg)	11.64	6.85
Initial inclination (deg)	0.00	0.00
Floquet Multiplier 1	1.000	1.000
Floquet Multiplier 2	1.000	1.000
Floquet Multiplier 3	1.000	1.000
Floquet Multiplier 4	1.000	1.000
Floquet Multiplier 5	$0.7531 + 0.6578 i$	$0.7023 + 0.7119 i$
Floquet Multiplier 6	$0.7531 - 0.6578 i$	$0.7023 - 0.7119 i$

Table 2. Approximate initial states for the bifurcation points where the Reflection and the Axial families branch from the Planar family. The set of Floquet multipliers for each case has two pairs of values +1, showing that each solution belongs to two families of periodic orbits.

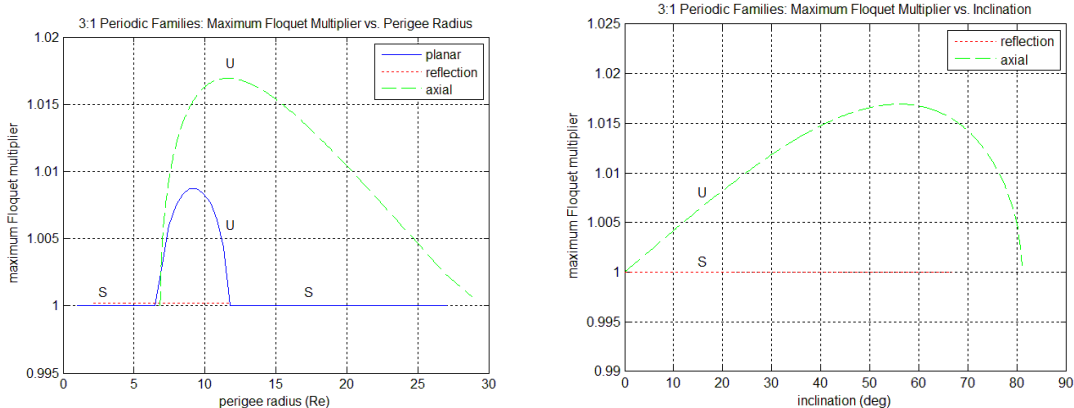


Figure 28. Maximum Floquet multiplier magnitudes for the periodic solutions. The left plot shows the maximum multiplier vs. perigee radius. The right plot shows the maximum multiplier vs. inclination for Reflection and Axial families. In each plot the red dotted line for the Reflection family was plotted slightly above its actual height of 1 to make it more visible. The fact that the maximum Floquet multiplier for the Axial branch approaches 1 for increasing perigee radius and inclination indicates that the branch is approaching another bifurcation point.

We have noted that the Planar Mirror family and the entire Axial family is spectrally unstable. However, as shown in Figure 28, even for the spectrally unstable solutions the maximum Floquet multiplier does not rise above about 1.017 per lunar cycle for the Planar or Axial families, so in twenty years a perturbation would not grow by more than a factor of $1.017^{267.6} = 91$. Moreover, the orbit where the Axial branch becomes vertical appears to be still another bifurcation point, as noted in the caption to Figure 28.

The computation of families of periodic orbits provides a variety of starting points for a mission trajectory design. For each periodic orbit we can use properties such as orbit shape, orbit period, the apsidal rotation in selecting an orbit. One can also use the linear analysis to identify the quasi-periodic solutions around a given periodic solution.

It is intriguing that the bifurcation diagram for families of nearly 3:1 resonant solutions in the CR3BP has some structure in common with bifurcation diagram for some families of libration point orbits shown in [14] and [25]. The Reflection resonant orbits exhibit the same mirror symmetry as the libration point Halo orbits; the Axial resonant orbits exhibit the same axial symmetry as the libration point Axial or “Y” libration point orbits; and the Planar Mirror resonant orbits share both symmetries with the Lyapunov libration point orbits. Moreover, the libration point orbits have a bifurcation diagram similar to the one shown above for the resonant orbits: The families of Halo orbits and the Axial / “Y” orbits each branch from the Lyapunov orbits at different points. The analogy between the two bifurcation diagrams may shed further light on both sets of families of periodic solutions.

The Lidov-Kozai Mechanism

We observed above that the quasi-periodic oscillations in the IBEX orbit, as well as those around the Reflection periodic orbit, exhibit two time scales: one on the order of 10 months, and a second on the order of 17 years. It appears that the long-period oscillation is connected with the Kozai resonance

mechanism, also called the Lidov-Kozai mechanism [40-41]. The Lidov-Kozai mechanism is believed to play a significant role in the evolution of extrasolar planetary systems [26] and triple star systems [27]. Ely [28] noted that the Lidov-Kozai mechanism also describes the Earth gravitational perturbation on lunar orbiters. The derivation of the Lidov-Kozai model begins by averaging out short-term oscillations. The model predicts that both the semimajor axis a and the quantity

$$(7) \quad H_K = \sqrt{1 - e^2} \cos(i)$$

are constant. The quantity $\sqrt{a}H_K$ is one of the Delaunay variables and represents the z component of orbital angular momentum [13] [13]. The preservation of H_K is also connected with the Tisserand criterion in equation (4), since the semimajor axis is constant. It follows that, for prograde orbits, if eccentricity increases then inclination decreases, and vice versa. Put another way, the inclination and perigee radius vary in unison. We observe this behavior in Figure 17 and Figure 18 for the Reflection periodic solution. (Even for the unstable Planar Mirror and Axial solutions, Figure 15 and Figure 21 show that the perigee radius and inclination vary together.) Mazeh and Shaman [27] give an approximate period of the Lidov-Kozai oscillation:

$$(8) \quad P_K \approx P_2 \left(\frac{m_1 + m_2}{m_3} \right) \left(\frac{a_3}{a_2} \right)^3.$$

In expression (8), P represents period, m represents mass and a represents semimajor axis, while for our application the subscripts 1, 2 and 3 represent the Earth, spacecraft and Moon, respectively. To derive expression (8), terms on the order of unity were neglected, so (8) represents an order-of-magnitude approximation. Entering the relevant values in expression (8) we obtain an approximate Kozai period of 18.5 years, which agrees with the oscillation period for mode Q2 of 16.9 years found for the Reflection orbit in Figure 17 and Figure 18. Moreover, for all Reflection orbits with inclinations from 15 deg to 67 deg, the mode Q2 oscillation period ranges from 37 years down to 9 years. These periods are within a factor of 2 of the approximation (8). This strongly suggests that the Lidov-Kozai mechanism is connected with the long-term oscillations of the Reflection periodic orbits.

However, care must be taken when attempting to apply the Lidov-Kozai mechanism to near-resonance orbits such as IBEX. The derivation of the Lidov-Kozai model assumes that one can average out short-term oscillations. That assumption is not valid near a Mean Motion Resonance, such as the 3:1 resonance of IBEX. The Lidov-Kozai mechanism predicts qualitatively different evolution for the eccentricity and argument of perigee, depending on whether inclination is above or below a certain critical inclination that depends on the semimajor axis. Those predictions are not consistent with our bifurcation analysis, where stability of the Reflection and Axial solutions does not change with inclination. Moreover, the Lidov-Kozai mechanism does not apply directly to the IBEX orbit because IBEX is significantly affected by the Sun as well as the Moon. Thus while Figure 4 and Figure 5 show that the IBEX perigee radius and ecliptic inclination generally trend together, the two plots do not vary in unison. There have been studies of asteroid motion, such as [29] by Moons and Morbidelli, that consider secular resonances for asteroids near the 3:1 resonance in the context of a four-body problem (Sun-Jupiter-Saturn-asteroid). Such analysis may shed light on the spacecraft orbital dynamics near mean motion resonance in the Earth-Moon-Sun-spacecraft problem.

Propagation of an IBEX Orbit State in the CR3BP

We began this study to gain some understanding of the IBEX orbit dynamics exhibited in Figures 1 to 5. We have examined the dynamics of similar, near-resonant orbits in the CR3BP because it can offer insights through a simplified system that only models the gravitational effects of the Earth and the Moon, although the CR3BP cannot capture the full dynamics. To see how well the CR3BP dynamics capture the actual orbit dynamics of IBEX, it is useful to take an initial state from the IBEX orbit, transform it into CR3BP coordinates and propagate it using CR3BP dynamics. We can then compare the long-term behavior to that seen in Figures 1 to 5 for a high-fidelity force model. At 23 April 2013 00:00:00 UTC, the J2000 position of IBEX was (242993.633409, -34985.396684, 52286.448539) km and the velocity was (-0.507391, 0.883484, 0.094170) km/sec. Using the state of the Moon at that epoch, we transformed this initial state to obtain a CR3BP position (-0.6546, -0.0126, 0.1162) and velocity (0.5619, -0.1561, -0.1723).

Figure 29 shows the evolution of the semimajor axis under CR3BP dynamics. Figure 29 is comparable to Figure 3, which shows the evolution in a high-fidelity force model. We see that the semimajor axis in both plots oscillates about a constant value of about 28.9 Earth radii. The range of semimajor axis values in Figure 29 is similar to the range in Figure 3, but slightly smaller. The oscillation in Figure 29 exhibits a period of about 9 months, close to but slightly longer than the oscillation in Figure 3. In addition, Figure 3 exhibits more variability than Figure 29, which is to be expected since Figure 3 includes the effects of the Sun's gravity and other forces.

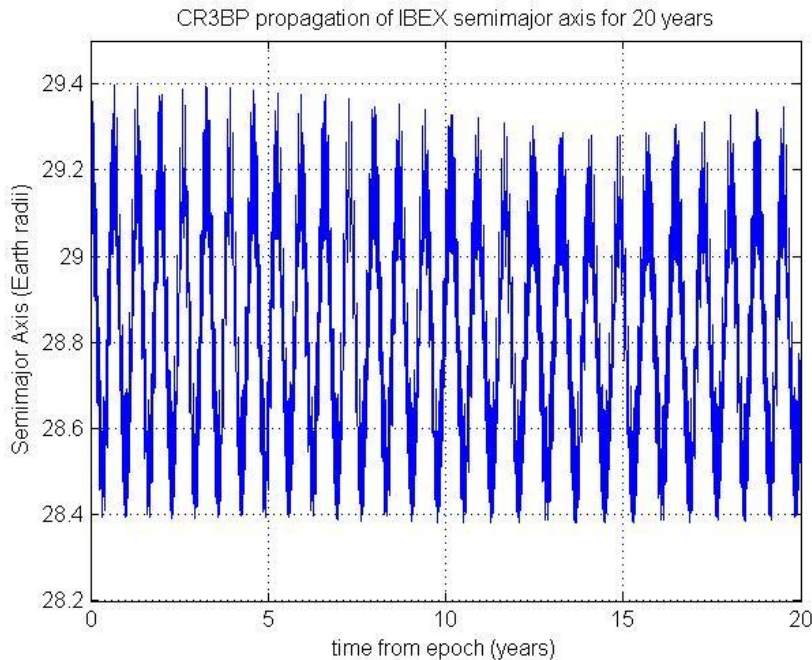


Figure 29. Twenty year evolution of IBEX semimajor axis under CR3BP dynamics. The range of values is comparable to those in Figure 3, but slightly smaller. The plot exhibits an oscillation with period near 9 months, slightly longer than the oscillation seen in Figure 3.

Figures 30 and 31 show the evolution of the perigee radius and inclination from the lunar orbit plane, respectively, under CR3BP dynamics. It is apparent that the perigee radius and inclination oscillate in unison, with a period of about 24 years, consistent with the Lidov-Kozai mechanism. Figures 30 and 31 can be compared to Figures 4 and 5, respectively, for the high-fidelity force model. The CR3BP model

captures some of the same dynamic features as the high-fidelity model: a medium-term oscillation with period around 9 months, and a long-term oscillation with a period of decades.

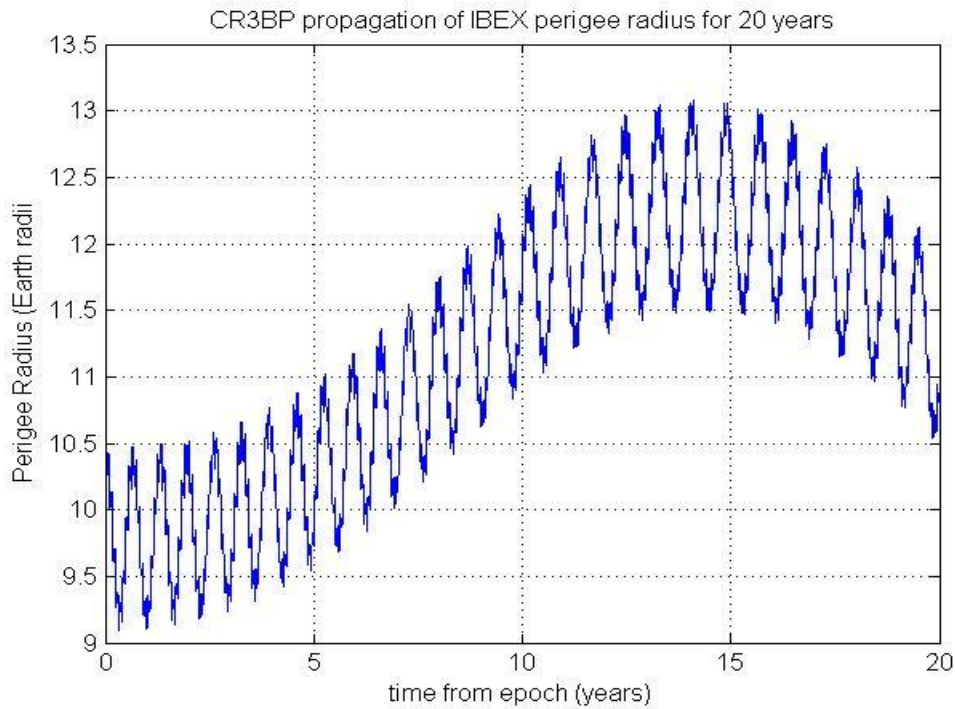


Figure 30. Twenty year evolution of IBEX perigee radius under CR3BP dynamics.

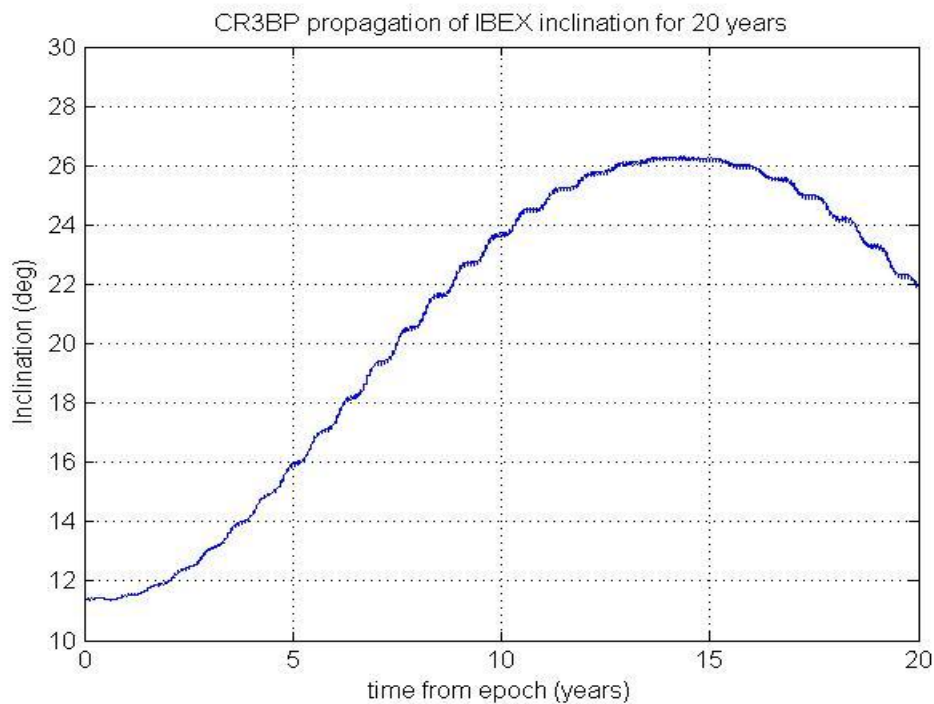


Figure 31. Twenty year evolution of IBEX inclination from the lunar orbit plane, under CR3BP dynamics.

However, it is also apparent that the two models show remarkably different long-term evolution. In particular, thirteen years after the epoch, the high-fidelity model predicts perigee radius and inclination will be near minimum values of about 6 Re and 11 deg, respectively, whereas the CR3BP model predicts perigee radius and inclination will be near maximum values of about 13 RE and 26 deg, respectively. The key factor that is missing from the CR3BP dynamics is the gravity of the Sun. The Sun's gravity affects the evolution of inclination from the lunar orbit plane in two ways: There is a direct effect on the motion of the satellite itself, and an indirect effect as the Sun's gravity causes the lunar orbit plane to evolve with a period of 18.6 years. (See [30], p. 281.) In an analysis of the dynamics of the TESS mission orbit near 2:1 resonance [31], we demonstrated that by including the Sun's gravity in a Bi-circular restricted 4-body problem, we can achieve much better agreement with the high-fidelity propagation. However such a model lacks the elegance of the CR3BP that makes it so well suited as a starting point in the design of mission where multibody dynamics are important. Time appears explicitly in the dynamics of the 4-body problem, and we generally cannot compute continuous families of periodic orbits.

Conclusions and Future Work

The goal of this study was to understand better the dynamics of the IBEX extended mission orbit and its apparent long-term stability. Toward this end we have examined, in the context of the Circular Restricted 3-Body Problem, three types of near 3:1 resonant periodic orbits in the Earth-Moon system that are similar to the IBEX orbit: Planar Mirror, Reflection and Axial orbits. The results are summarized in Table 3.

We first studied these periodic solutions using Floquet theory to assess local stability, and then extended the analysis with long-term propagations of perturbations along each of the Floquet modes. The Reflection solution is spectrally stable. Although the Planar Mirror solution and Axial solution are spectrally unstable, the instability is so mild that it has little practical effect over twenty years. The Lidov-Kozai mechanism helps to describe the long-term quasi-periodic oscillations observed in the orbit elements, but that model does not consider mean motion resonance and so does not apply completely in our study. The Poincaré maps showed that all three solutions appear stable for twenty years under perturbations more than a thousand times larger than the IBEX orbit determination errors. This makes near-resonant orbits very attractive for space missions using small spacecraft with limited propellant budgets.

We also generated bifurcation diagrams of these families of solutions. The bifurcation diagram provides a broader understanding of the near-resonant solutions, and offers the mission designer a wider range of choices. Using one of the periodic solutions shown above, Randy Paffenroth of Numerica Corporation has used the AUTO numerical continuation software to compute a more complete bifurcation diagram for the near-resonant families, and has found further bifurcations [32].

We concluded the analysis by examining the evolution of an IBEX initial state under CR3BP dynamics. In the CR3BP model, semimajor axis in Figure 29 oscillates with period near 9 months and shows no secular growth, similar to the behavior for the high-fidelity force model in Figure 3. Perigee radius and inclination in Figure 30 and Figure 31 show oscillations with period near 9 months and near 24 years. Perigee radius and inclination vary in unison with large amplitude in the long-period oscillation,

consistent with the Lidov-Kozai mechanism. Perigee radius and inclination evolution under the high-fidelity model in Figure 4 and Figure 5 show more complex features, due to the Sun’s gravity on the spacecraft and the Moon.

	Planar Mirror	Reflection	Axial
Analogous Libration Point Orbit family	Lyapunov	Halo	Axial
Design parameter used, comparable to IBEX orbit	Apogee radius = 49.95 Re	Inclination to lunar orbit plane = 23 deg	Inclination to lunar orbit plane = 23 deg
Floquet theory analysis to determine multipliers and modes (Figures 6 to 12, and Table 1)	One quasiperiodic pair, with period 222 days Unstable component grows by factor of 10 in 8090 days	One quasiperiodic pair, with period 272 days One quasiperiodic pair, with period 6167 days	One quasiperiodic pair, with period 222 days Unstable component grows by factor of 10 in 6719 days
Floquet mode propagation, with perturbation magnitude comparable to orbit determination error (Figures 13 to 22)	Semimajor axis shows quasiperiodic motion but very slow growth Perigee radius and inclination show quasiperiodic and stable/unstable components with time scales matching Floquet multipliers	Semimajor axis shows quasiperiodic motion Perigee radius and inclination show quasiperiodic with time scales matching Floquet multipliers	Semimajor axis shows quasiperiodic motion but very slow growth Perigee radius and inclination show quasiperiodic and stable/unstable components with time scales matching Floquet multipliers
Poincaré section analysis, with perturbation magnitude comparable to orbit determination error (Figures 23 to 25)	Twenty year propagation with perturbations on order of orbit determination error demonstrates effective stability, and quasiperiodic oscillations	Twenty year propagation with perturbations on order of orbit determination error demonstrates effective stability, and quasiperiodic oscillations	Twenty year propagation with perturbations on order of orbit determination error demonstrates effective stability, and quasiperiodic oscillations
Bifurcation analysis (Figures 26 to 28, and Table 2)	Orbits are mildly unstable for perigee radius between 6.85 and 11.64 Re, otherwise spectrally stable	All orbits are spectrally stable. Family branches from Planar Mirror family at perigee radius 11.64 Re, then perigee radius decreases with increasing inclination	All orbits are mildly unstable. Family branch from Planar Mirror family at perigee radius 6.85 Re, then perigee radius increases with increasing inclination until vertical circular orbit in inertial frame
Evolution of IBEX state under CR3BP dynamics (Figures 29 to 31)	Semimajor axis shows no secular growth, and oscillates with period of about 9 months, similar to high-fidelity dynamics. Perigee radius and inclination show two oscillations with periods near 9 months and 24 years. Perigee radius and inclination oscillate in unison, with large amplitude, consistent with Lidov-Kozai mechanism. High-fidelity dynamics exhibit more complex features, due to Sun’s gravity on the spacecraft and on the Moon.		
Practical stability	Over the course of a decade-long mission, it would be difficult to distinguish long-term oscillations from slow-growth instability. Either case would produce practical orbit stability, with few or no orbit maintenance maneuvers required.		

Table 3. Summary of analysis results for the three families of resonant orbits in the CR3BP, and for IBEX orbit evolution under CR3BP dynamics and high-fidelity dynamics.

The CR3BP can be a useful tool for understanding the dynamics of a resonant orbit. It allows us to capture the qualitative evolution of semimajor axis, perigee radius and inclination, including the oscillation of the least two in unison. The CR3BP also allows us to compute families of periodic resonant orbits, much as the CR3BP has been used to compute families of Libration Point Orbits. However we have seen that the CR3BP does not capture the orbit evolution accurately, primarily because it neglects the Sun’s gravity on the spacecraft and on the Moon. The TESS mission orbit will be near 2:1 resonance with the Moon. In a study of the TESS orbit similar to this one [31], we included the Sun’s gravity using a

Bi-circular Restricted 4-Body Problem (BCR4BP), and achieved good agreement with the high-fidelity force model for the duration of a four-year mission.

There are several directions for future work in this area. Like our study of the TESS orbit, we can use the BCR4BP to study other resonant orbits. The present study has focused on periodic solutions, but it is clear that the IBEX orbit is a quasiperiodic solution, so quasi-periodicity deserves further attention. We have not yet addressed how to reach a resonant orbit, but Vaquero and Howell have investigated transfer between resonance orbits via invariant manifolds [27-29]. Works such as [29] on asteroid motion may help us to understand better spacecraft orbit dynamics near a mean motion resonance. In particular, while the Lidov-Kozai mechanism appears to describe the long-term oscillations in these orbits, we do not yet have a model for the oscillations with period near 9 months.

The present study has focused on 3:1 resonant solutions. It would be interesting to examine orbits near 2:1 and 4:1 resonance, both of which we considered for the IBEX extended mission orbit [1] and may be useful in future missions. In [31] we have generated a bifurcation diagram for the 2:1 periodic orbits, and found that near the Planar family the bifurcation diagram for the 2:1 case is very similar to the 3:1 case. However the global behavior of the 2:1 Axial branch appears distinctly different from the 3:1 case: We did not find a bifurcation point in the 2:1 Axial family until the inclination reached 180 deg, where the orbit is circular. Finally, it would be intriguing to pursue the analogy between resonance orbits and libration points orbits in the CR3BP.

Acknowledgements

This research was performed at Applied Defense Solutions and was supported in part by a contract with the Southwest Research Institution (SwRI). The authors thank Mark Tapley of SwRI, Trevor Williams of NASA Goddard and an anonymous reviewer for their valuable comments. We thank Kathleen Howell and Mar Vaquero at Purdue University for sharing their research into resonance orbits. We thank George Ricker at MIT and our colleagues at the NASA Goddard Navigation and Mission Design Branch for pointing us to the Lidov-Kozai mechanism. DJD thanks Randy Paffenroth at Numerica Corporation for valuable discussions on the structure of the bifurcation diagram.

Bibliography

- [1] J.P.Jr. Carrico et al., "Lunar-Resonant Trajectory Design for the Interstellar Boundary Explorer (IBEX) Extended Mission," in *AAS/AIAA Astrodynamics Specialist Conference*, Girdwood AK, 2011.
- [2] H. Poincare, *New Methods in Celestial Mechanics*. New York: American Institute of Physics, 1993.
- [3] H.W. Broer, G.B. Huitema, and M.B. Sevryuk, *Quasi-Periodic Motions in Families of Dynamical Systems: Order amidst Chaos, Vol. 164*. Berlin: Springer-Verlag, 2002.
- [4] J.D. Hadjidemetriou, "Resonant Motion in the Restricted Three Body Problem," *Celestial Mechanics and Dynamical Astronomy*, vol. 56, pp. 201-219, 1993.

- [5] J. Henrard and N.D. Caranicolas, "Motion Near the 3/1 Resonance of the Planar Elliptic Restricted Three-Body Problem," *Celestial Mechanics and Dynamical Astronomy*, vol. 47, pp. 99-121, 1993.
- [6] R.A. Broucke, "Periodic Orbits in the Restricted Three-Body Problem with Earth-Moon Masses," 1968.
- [7] MIT. (2013, April) MIT News: NASA selects MIT-led TESS project for 2017 mission. [Online]. <http://web.mit.edu/newsoffice/2013/nasa-selects-tess-for-mission-0405.html>
- [8] A.E. Roy and M.W. Ovenden, "On the Occurrence of Commensurable Mean Motions in the Solar System II. The Mirror Theorem," *Monthly Notices of the Royal Astronomical Society*, pp. 296-309, 1955.
- [9] K.A. Howell, "Three-Dimensional Periodic 'Halo' Orbits," *Celestial Mechanics*, vol. 32, pp. 53-71, 1984.
- [10] D.J. McComas et al., "A new class of long-term stable lunar resonance orbits: Space Weather applications and the Interstellar Boundary Explorer," *Space Weather*, 2011.
- [11] K. R. Meyer, *Periodic Solutions of the N-Body Problem*. New York: Springer, 1999.
- [12] J. Danby, *Fundamentals of Celestial Mechanics*. Richmond: Willmann-Bell, 1988.
- [13] C.D. Murray and S.F. Dermott, *Solar System Dynamics*. Cambridge: Cambridge University Press, 2000.
- [14] D.J. Dichmann, E.J. Doedel, and R.C. Paffenroth, "Computation of Periodic Solutions of the 3-Body Problem Using the Numerical Continuation Software AUTO," in *Libration Point Orbits and Applications*, 2003, pp. 489-528.
- [15] E.J. Doedel et al., "Computation of Periodic Solutions of Conservative Systems with Application to the 3-Body Problem," *International Journal of Bifurcation and Chaos*, vol. 13, no. 6, pp. 1353-1382, June 2003.
- [16] K.R. Meyer and G.R. Hall, *Introduction to Hamiltonian Dynamics and the N-Body Problem*. New York: Springer, 1992.
- [17] C. Marchal, *The Three-Body Problem*. New York: Elsevier, 1990.
- [18] W.E. Wiesel and D.J. Pohlen, "Canonical Floquet Theory," *Celestial Mechanics and Dynamical Astronomy*, vol. 58, pp. 81-96, 1994.
- [19] R. Miller and A. Michel, *Ordinary Differential Equations*. New York: Academic Press, 1982.

- [20] G.E. Shilov, *Linear Algebra*. New York: Dover, 1977.
- [21] K.A Howell and J. Keeter, "Station-keeping Strategies for Libration Point Orbits: Target Point and Floquet Mode Approaches," in *Proceedings of the AAS/AIAA Spaceflight Mechanics Conference 1995, Advances in the Astronautical Sciences, Vol. 89*, vol. 89, 1995, pp. 1377-1396.
- [22] T.S. Parker and L.O. Chua, *Practical Numerical Algorithms for Chaotic Systems*. New York: Springer-Verlag, 1989.
- [23] M. Vaquero and K.C. Howell, "Poincaré Maps and Resonant Orbits in the Circular Restricted Three-Body Problem," in *AAS 11-428*, 2011.
- [24] R. Seydel, *Practical Bifurcation and Stability Analysis from Equilibrium to Chaos*. New York: Springer, 1994.
- [25] E.J. Doedel, V.A. Romanov, R.C Paffenroth, H.B. Keller, and D.J. Dichmann, "Elemental Periodic Orbits Associated with the Libration Points in the Circular Restricted 3-Body Problem," *International Journal of Bifurcation and Chaos*, vol. 17, no. 8, pp. 2625-2677, 2007.
- [26] G. Takeda and F.A. Rasio, "High Orbital Eccentricities of Extrasolar Planets Induced by the Kozai Mechanism," *Astrophys. J.*, vol. 627, pp. 1001-1010, 2005.
- [27] T. Mazeh and J. Shaman, "The Orbital Evolution of Close Triple Systems: The Binary Eccentricity," *Astron. Astrophys.*, vol. 77, pp. 145-151, 1979.
- [28] T. Ely, "Stable Constellations of Frozen Elliptical Inclined Lunar Orbits," *J. Astronautical Sci.*, vol. 53, no. 3, pp. 301-316, 2005.
- [29] M. Moons and A. Morbidelli, "Secular Resonance in Mean Motion Commensurabilities: The 4/1, 3/1, 5/2 and 7/3 Cases," *Icarus*, vol. 114, pp. 33-50, 1995.
- [30] A. Roy, *Orbital Motion*. Bristol: Adam Hilger, 1988.
- [31] D. Dichmann, *Dynamical Systems Analysis of TESS Mission Orbit*, 2012.
- [32] R.C. Paffenroth, Private Communication, June 2011.
- [33] R Lebois, L. Policastri, J.P.Jr. Carrico, and M. Intelisano, "Extended Mission Maneuver Operations for the Interstellar Boundary Explorer (IBEX)," in *AAS/AIAA Space Flight Mechanics Meeting*, Charleston, SC, 2012.
- [34] J. Wisdom, "A perturbative treatment of motion near the 3/1 commensurability," *Icarus*, vol. 63, pp. 272-289, 1985.

- [35] G. Voyatzis, "Chaos, Order and Periodic Orbits in 3:1 Resonant Planetary Dynamics," *Astrophysical J.*, vol. 675, pp. 802-816, 2008.
- [36] J.S. Parker and M.W. Lo, "Unstable Resonant Orbits near Earth and Their Applications in Planetary Missions," in *AIAA/AAS Astrodynamics Specialist Conference*, Providence, RI, 2004.
- [37] D.V. Byrnes, J.M. Longuski, and B. Aldrin, "Cycler Orbits between Earth and Mars," *J. Spacecraft and Rockets*, vol. 30, pp. 334-336, 1993.
- [38] S.J. Peale, "Orbital Resonances in the Solar System," in *Annual review of astronomy and astrophysics. Volume 14.*, 1976, pp. 215-246.
- [39] M. Lidov, "The Evolution of Orbits of Artificial Satellites of Planets under the Action of Gravitational Perturbations of External Bodies," *Planet. Space Sci.*, vol. 9, pp. 719-759, 1962.
- [40] Y. Kozai, "Secular Perturbations of Asteroids with High Inclination and Eccentricity," *Astron. J.*, vol. 9, pp. 591-598, 1962.
- [41] M. Mathews, M. Hametz, J. Cooley, and D. Skillman, "High Earth Orbit Design for Lunar Assisted Small Explorer Missions," in *NASA GSFC Flight Mechanics and Estimation Theory Symposium*, Greenbelt, MD, 1994.
- [42] D. McGiffin, M. Mathews, and S. Cooley, "High Earth Orbit Design for Lunar-Assisted Medium Class Explorer Missions," in *NASA GSFC Flight Mechanics Symposium*, Greenbelt, MD, 2001.
- [43] J. Laskar and A.C.M. Correia, "HD69532, a planetary system in a 3:1 mean motion resonance," *Astronomy and Astrophysics*, vol. 496, pp. 15-18, 2009.
- [44] M. Vaquero and K.C. Howell, "Design of Transfer Trajectories between Resonant Orbits in the Restricted Problem with Applications to the Earth-Moon System," in *1st IAA Conference on Dynamics and Control of Space Systems*, Porto, Portugal, 2012.
- [45] M. Vaquero and K.C. Howell, "Leveraging Resonant Orbit Manifolds to Design Transfers between Libration Point Orbits in Multi-body Regimes," , 2013.
- [46] F. Brauer and J. Nohel, *The Qualitative Theory of Ordinary Differential Equations*. New York: Dover, 1969.
- [47] J. Hadjidemetriou, "Periodic orbits in gravitational systems," in *Chaotic Worlds: From Order to Disorder in Gravitational N-Body Dynamical Systems*, B.A. Steves, A.J. Maciejewski, and M. Hendry, Eds. New York: Springer, 2006, pp. 43-80.
- [48] R. Dvorak, "New Results on the Motions of Asteroids in Resonances," in *Chaos, Resonance and*

Collective Dynamical Phenomena in the Solar System. Dordrecht: Kluwer Academic, 1992, pp. 145-152.

[49] S. Ferraz-Mello, "Kirkwood Gaps and Resonant Groups," in *Asteroids, Comets, Meteors*. New York: Springer, 1994, pp. 175-188.

Appendix

The CR3BP system (1) can be written concisely as

$$(A.1) \quad \mathbf{s}' = \mathbf{f}(\mathbf{s}) = \mathbf{K} \left(\frac{\partial H}{\partial \mathbf{s}} \right)^T$$

where $\frac{\partial H^T}{\partial \mathbf{s}} = \left(\frac{\partial H}{\partial \mathbf{r}}, \frac{\partial H}{\partial \mathbf{v}} \right)^T$ is the derivative of the Hamiltonian $H(\mathbf{s}) = -C(\mathbf{s})/2$, and $C(\mathbf{s})$ is the Jacobi integral given by equation (2). The 6-by-6 skew-symmetric matrix \mathbf{K} is given by

$$\mathbf{K} = \begin{pmatrix} \mathbf{0} & \mathbf{I} \\ -\mathbf{I} & 2\mathbf{J}_2 \end{pmatrix}$$

where $\mathbf{0}$ is the 3-by-3 zero matrix, \mathbf{I} is the 3-by-3 identity matrix, and

$$\mathbf{J}_2 = \begin{pmatrix} 0 & 1 & 0 \\ -1 & 0 & 0 \\ 0 & 0 & 0 \end{pmatrix}.$$

Equation (A.1) is a nonstandard Hamiltonian system. In a standard (or canonical) Hamiltonian system, the block matrix in the lower right of matrix \mathbf{K} would be $\mathbf{0}$. It is also possible to express the CR3BP as a standard Hamiltonian system, where the velocity is replaced by momentum variables in the state vector [11].

Let $\mathbf{s}(t, \mathbf{s}_0)$ be the solution of equation (A.1) with state \mathbf{s}_0 at time $t = 0$. Let $\Phi(t, \mathbf{s}_0)$ be the state transition matrix (or fundamental matrix) for system (A.1), so that $\Phi(t, \mathbf{s}_0)$ is the derivative of the solution with respect to the initial state. That is, $(t, \mathbf{s}_0) = \partial \mathbf{s}(t, \mathbf{z}) / \partial \mathbf{z} |_{\mathbf{z}=\mathbf{s}_0}$. The matrix $\Phi(t, \mathbf{s}_0)$ satisfies the differential equation

$$(A.2) \quad \Phi' = \mathbf{Df}(\mathbf{s}(t, \mathbf{s}_0))\Phi, \quad \Phi(0, \mathbf{s}_0) = \mathbf{I}$$

Equations (1) and (A.2) together define a system of 42 first-order differential equations for state \mathbf{s} and state transition matrix Φ . We sometimes suppress the dependence of Φ on the initial state for brevity. Because the system (A.1) is Hamiltonian,

$$(A.3) \quad D\mathbf{f}(\mathbf{s}) = \mathbf{K}D^2H(\mathbf{s})$$

where $D^2H(\mathbf{s}) = \partial^2H(\mathbf{s})/\partial^2\mathbf{s}$ is a symmetric matrix.

The state transition matrix satisfies the symplectic condition

$$(A.4) \quad \Phi^T \mathbf{K}^{-1} \Phi = \mathbf{K}^{-1}$$

Equation (A.4) is true at $t = 0$ because $(0, \mathbf{s}_0) = \mathbf{I}$. To complete the proof we can differentiate $\Phi^T \mathbf{K}^{-1} \Phi$ with respect to time, then employ equations (A.2) and (A.3) and the fact that \mathbf{K} is skew-symmetric. One implication of equation (A.4) is that $\det(\Phi(t)) = +1$ for all t , which implies that the product of eigenvalues of Φ equals $+1$. Because Φ is invertible, 0 is not an eigenvalue. Suppose $\Phi \mathbf{v} = \lambda \mathbf{v}$ where $\mathbf{v} \neq 0$. Because Φ is real-valued, $\Phi \bar{\mathbf{v}} = \bar{\lambda} \bar{\mathbf{v}}$ so the conjugate $\bar{\lambda}$ is also an eigenvalue. If we pre-multiply $\Phi \mathbf{v} = \lambda \mathbf{v}$ by $\Phi^T \mathbf{K}^{-1}$, it follows that $(\mathbf{K}^{-1} \mathbf{v})^T$ is a left eigenvector of Φ with eigenvalue $1/\lambda$. It follows that eigenvalues of Φ other than ± 1 occur in groups:

- A pair $(\lambda, 1/\lambda)$ where λ is real and $\lambda \neq 1$
- A pair $(\lambda, \bar{\lambda})$ where λ is complex and $|\lambda| = 1$
- A quadruplet $(\lambda, \bar{\lambda}, 1/\lambda, 1/\bar{\lambda})$ where λ is complex and $|\lambda| \neq 1$.

The first two of these cases are the most common.

Let $\mathbf{s}^P(t, \mathbf{s}_0^P)$ be a periodic solution of (1) with period T , and let $\mathbf{M} = \Phi(T)$ be the corresponding monodromy matrix. From Floquet theory, the state transition matrix can be expressed as

$$(A.5) \quad \Phi(t - t_0) = \mathbf{P}(t) \exp(\mathbf{B}(t - t_0)) \mathbf{P}(t_0)^{-1}$$

where $\mathbf{P}(t)$ is nonsingular with period T , and \mathbf{B} is a constant matrix. See, for example, [1], or [18]. The monodromy matrix \mathbf{M} is then given by $\mathbf{M} = \exp(\mathbf{B}T)$. Equation (A.5) shows that the evolution of a perturbation is governed by two distinct factors: The constant matrix \mathbf{B} in the exponent describes the long-term variation, and the periodic matrix $\mathbf{P}(t)$ describes the oscillation within a single period. For stability analysis, we are only concerned with the long-term behavior. Floquet theory implies that, to assess the linear stability of a periodic solution, it is sufficient to examine the eigenstructure of the monodromy matrix \mathbf{M} . As shown in [11] (Lemma 6.4.1, p. 77), because the dynamics (1) are time-independent, the state derivative $\mathbf{f}(\mathbf{s}_0^P)$ is a right eigenvector of \mathbf{M} with eigenvalue $+1$:

$$(A.6) \quad \mathbf{M} \mathbf{f}(\mathbf{s}_0^P) = \mathbf{f}(\mathbf{s}_0^P)$$

In addition, $\partial H/\partial \mathbf{s}$ is a left eigenvector of \mathbf{M} with eigenvalue $+1$. This fact is proved in [11] (Lemma 6.5.1, p. 80.). It also follows because $\mathbf{f}(\mathbf{s}_0^P) = \mathbf{K}(\partial H/\partial \mathbf{s})^T$ is a right eigenvector with eigenvalue $+1$, so $(\mathbf{K}^{-1} \mathbf{f}(\mathbf{s}_0^P))^T = \partial H/\partial \mathbf{s}$ is a left eigenvector with eigenvalue $+1$.

In a family of periodic solutions, the period generally depends on an integral of motion. In the case of Keplerian motion, the period of an orbit depends on the energy, but not on the angular momentum or the Runge-Lenz vector. Figure 27 shows that period depends on the Jacobi integral in each of the three families studied here. Wiesel [18], p. 84, notes that, if the period depends on an integral C , then \mathbf{M} must have a generalized eigenvector associated with eigenvalue +1: If \mathbf{v} be a vector along $\mathbf{f}(\mathbf{s}_0^P)$, then there exists a generalized eigenvector \mathbf{g} and a scalar τ such that

$$(A.7) \quad \mathbf{M}(\mathbf{f} \ \mathbf{g}) = (\mathbf{f} \ \mathbf{g}) \begin{pmatrix} 1 & \tau \\ 0 & 1 \end{pmatrix}$$

or

$$(A.8) \quad \mathbf{M} \mathbf{f} = \mathbf{f}$$

$$(A.9) \quad \mathbf{M} \mathbf{g} = \mathbf{g} + \tau \mathbf{f}$$

Moreover, a perturbation along \mathbf{g} perturbs the integral C and so perturbs the period. Equation (A.8) is a restatement of equation (A.6). Equation (A.9) also has a basic physical interpretation. Suppose that the initial state of the nominal periodic solution \mathbf{s}_0^P is perturbed a small amount along direction \mathbf{g} so that the integral C is perturbed slightly from the nominal. Then the period of the perturbed solution is also slightly different from the nominal solution, so after one period the perturbed solution will be offset by a small amount along the tangent direction. As noted above, this is precisely the behavior we see when a Keplerian orbit is perturbed in a way that changes the energy.

When we numerically compute the eigenvalue decomposition of monodromy matrix \mathbf{M} using the Matlab function *eig*, the eigenvalue +1 cannot be found precisely, due to finite precision. Instead Matlab can produce a pair of eigenvalues $1 + \varepsilon$ and $(1 + \varepsilon)^{-1} \approx 1 - \varepsilon$, with corresponding eigenvectors of the form $\mathbf{f} + \gamma \mathbf{g}$ and $\mathbf{f} - \gamma \mathbf{g}$, where $\varepsilon \ll 1$ and $\gamma \ll 1$. Therefore

$$(A.10) \quad \mathbf{M}(\mathbf{f} + \gamma \mathbf{g}) = (1 + \varepsilon)(\mathbf{f} + \gamma \mathbf{g}) = \mathbf{f} + \varepsilon \mathbf{f} + \gamma \mathbf{g} + \varepsilon \gamma \mathbf{g}$$

$$(A.11) \quad \mathbf{M}(\mathbf{f} - \gamma \mathbf{g}) = (1 - \varepsilon)(\mathbf{f} - \gamma \mathbf{g}) = \mathbf{f} - \varepsilon \mathbf{f} - \gamma \mathbf{g} + \varepsilon \gamma \mathbf{g}$$

If we neglect terms of order $\varepsilon \gamma$ in equations (A.10) and (A.11), and take the sum and the difference of these two equations, we obtain equations of the form (A.8) and (A.9), where $\tau = \varepsilon/\gamma$. Thus we can use the Matlab results to construct the generalized eigenvector. Rather than producing a pair of real eigenvalues near 1, Matlab *eig* can produce a complex conjugate pair of eigenvalues near +1. In that case, we can separate the real and imaginary pairs of the eigenvectors to obtain vectors \mathbf{f} and \mathbf{g} .